Monthly Notices of the ROYAL ASTRONOMICAL SOCIETY

MNRAS **531,** 4212–4237 (2024) https://doi.org/10.1093/mnras/stae1307
Advance Access publication 2024 May 25

Searching for OB-type pre-supernova binary companions inside supernova remnants

B. Dinçel,[1]★† M. Uzuner,[2,3] R. Neuhäuser,[1] A. Pannicke,[1] S. K. Yerli,[4] A. Ankay,[5] M. Mugrauer[1] and G. Torres[6]

[1]*Astrophysikalisches Institut und Universitäts-Sternwarte Jena, D-07745 Jena, Germany*
[2]*Faculty of Engineering and Natural Sciences, Sabancı University, Orhanlı-Tuzla, İstanbul 34956, Türkiye*
[3]*School of Physics and Astronomy, Cardiff University, Queen's Buildings, The Parade 5, Cardiff CF24 3AA, UK*
[4]*Orta Doğu Teknik Üniversitesi, Department of Physics, 06800 Ankara, Türkiye*
[5]*Boğaziçi University, Department of Physics, 34342 İstanbul, Türkiye*
[6]*Center for Astrophysics | Harvard & Smithsonian, 60 Garden Str, Mail Stop 20, Cambridge, MA 02138, USA*

Accepted 2024 April 29. Received 2024 March 8; in original form 2023 May 27

ABSTRACT

We searched for OB-runaway stars inside supernova remnants (SNRs) as a pre-supernova binary companion. As the majority of massive stars are found in close binary systems, a runaway star ejected by the orbital energy after the supernova (SN) is expected to be found. Considering a binary mass fraction, $q = 0.25-1.0$, the runaway star is likely to have an OB spectral type. We selected 12 SNRs at Galactic longitudes $109°-189°$. Using *Gaia* astrometry, we selected stars having consistent distances with those of the SNRs and showing a peculiar proper motion directed away from the central region of the SNRs. We also determined the radial distribution of the extinction towards the SNRs and estimated the spectral types of the OB-runaway candidates through *Gaia* and Two Micron All Sky Survey photometry. We found two candidates among 12 SNRs. By spectroscopic observations, *Gaia* DR3 1956321525606214 40 inside SNR G166.0 + 4.3 was found to be an evolved A3 type star that cannot be the pre-SN binary companion to the progenitor. *Gaia* DR3 5139277507673758 72 inside SNR HB 3 is the only OB-runaway candidate (2D space velocity of 33.3 ± 3.3 km s^{-1}). Based on photometric study, the star can be an early B-type main-sequence star with a slightly higher extinction relative to the SNR; however, it might instead be an evolved A-type star at the same distance. The other 11 SNRs do not host an OB-runaway star within their central regions. Although the runaway search was performed in a large interval of distance and extinction, we also estimated distances to the SNRs.

Key words: ISM: supernova remnants – stars: early-type.

1 INTRODUCTION

High space velocities of OB-runaway stars are explained by two independent mechanisms: dynamical ejection due to gravitational interactions of massive stars in cluster cores (Poveda, Ruiz & Allen 1967) and binary disruption as a result of a supernova (SN) explosion of the initially more massive component (Blaauw 1961). Both scenarios are viable, but whether one of the mechanisms is dominant is still uncertain. The asymmetry in SN explosions can give a high kick velocity to the neutron star (NS; Wongwathanarat, Janka & Müller 2013). This is confirmed by high space velocities measured for pulsars (300–500 km s^{-1}) (Lyne & Lorimer 1994, Allakhverdiev et al. 1997, Hobbs et al. 2005). Although a group of NS with low space velocities exists (Arzoumanian, Chernoff & Cordes 2002), most of the pulsars are found in isolation implying that the high kick mechanism is dominant. Also, the majority of the OB-runaway stars are not known to be multiple stars (Sayer, Nice & Kaspi 1996). According to the virial theorem, if less than half of the total mass of the system is released, then the new-born NS (or black hole) and the companion remain gravitationally bound (Blaauw 1961). So, if the compact object does not receive a significant kick and the majority of the total mass is stored on the secondary through conservative mass transfer, binary disruption does not occur (van den Heuvel 1993; van den Heuvel & van Paradijs 1997). The runaway high-mass X-ray binaries like 4U1700-37 (Ankay et al. 2001), Vela X-1 (Kaper et al. 1997), and 4U 2206 + 54 (Hambaryan et al. 2022) are such examples. Taking into consideration the selection effects, the low rate of X-ray binaries and the high rate of isolated neutron stars implies that the binary disruption is likely to occur in most cases (Guseinov, Ankay & Tagieva 2005, hereafter G05). According to Renzo et al. (2019), 78^{+9}_{-22} per cent of all massive star binaries do not merge, and 86^{+10}_{-22} per cent of these are disrupted by the binary SN.

Although the pre-SN companion can also be a less massive star, it is observationally more difficult to detect and to prove the runaway nature. Long lifetime and abundance in number increase their possibility of chance projection. Owing to their short lifetime,

★ E-mail: baha.dincel@uni-jena.de
† Former member

OB-type stars are relatively young objects; hence, their peculiar velocity can be detected easily by comparison with the velocity of the main body of the complex (birth site). Also, considering a mass ratio of 1:4–1:3, the companion to an SN progenitor would be expected as an OB-type star of which the effective temperature $T_{\rm eff}$ is larger than 10 000 K. In Lux et al. (2021), binary SN runaway stars from all spectral types have been searched in a sample of 12 supernova remnants (SNRs) that are thought to be rather nearby (<1−2 kpc). However, no very good candidate was found even though the spectra of six candidates showed Li 6708 Å line, which is proof of young age.

The kinematics of the binary disruption due to an asymmetric SN explosion is widely discussed in Tauris & Takens (1998). However, a sample of observationally confirmed OB-runaway-NS couples is needed for a better understanding of the problem. Therefore, we search for OB-runaway stars near the geometrical centres of SNRs that are the remnants of the companion star of the OB runaway.

Exploring OB-runaway stars inside SNRs provides us with valuable information. First, identifying the explosion centres more precisely will be useful for determining the kick direction and velocity of young NSs, thus the asymmetry of the SN. Secondly, the properties of the progenitor star can be found, therefore the origin of certain types of NSs and SNRs can be clarified. Thirdly, possible effects of a close binary system on the asymmetry of the SNe can also be examined. Lastly, SNR distance estimations have high uncertainty. As the OB-runaway star cannot move far away from the explosion centre in the observational lifetime of the SNR, the distance to the SNR can measured precisely using the parallax of the OB-runaway star.

In van den Bergh (1980), the kinematical study of known OB stars inside SNRs was concluded with a lack of OB-runaways due to the poor sample of SNRs and OB stars. The observational efforts in the CCD era are concentrated on runaway-NS coupling and abundance investigations of runaway stars. Some examples of the runaway-NS pairs (components are separated) are PSR1706 − 16 - ζ Oph (Neuhäuser, Gießler & Hambaryan 2020), and PSR J0826 + 2637–HIP 13962 (Tetzlaff et al. 2014). Based on their motions in space, the pulsars and the corresponding runaway stars were traced back in time by using 3D Monte Carlo simulations. They were found at the same position and the same time inside a young open cluster.

As the SN events took place more than 10^5 yr ago in these cases, the uncertainties are high. The SNR has faded away long ago and the separation between the objects is very large. Other important observational evidence is detecting the enhancement of α-process elements on the photosphere of the runaway stars. The photosphere of the hypervelocity star HD 271791 was found to be enriched in elements which can be synthesized in large amounts during the evolution of the progenitor. The viable explanation is that the material was ejected by the SN in the binary system (Przybilla et al. 2008).

By a systematic search for the OB-runaway stars inside the SNRs, we found an OB-runaway star, HD 37424, inside SNR S 147, and proved that the star was ejected by the binary disruption due to the SN of the progenitor of S 147 and the pulsar PSR J0538 + 2817, the kinematic study shows that the OB-runaway star and the pulsar was once at the same position in the space at the same time 30 ± 4 kyr (Dinçel et al. 2015). The zero-age main sequence progenitor mass should be greater than 13 $M_\odot$. Binary parameters were calculated for different progenitor masses. The Roche lobe radii suggest that it was an interacting binary in the late stages of the progenitor. The distance to the SNR is 1333^{+103}_{-112} pc and the extinction is 1.28 ± 0.06 mag. PSR J0538 + 2817 shows a characteristic age of 620 kyr, much higher than the kinematic age we found, 30 ± 4 kyr. The pulsar must have had a large initial spin period of $P_0 = 139$ ms (Kramer et al. 2003). So, we showed that such an NS indeed originated from the SN of a massive star (>13 $M_\odot$) in a close binary. Therefore, we have achieved our purposes by finding an OB-runaway star inside an SNR. *Gaia* astrometry has also confirmed that the distance of HD 37424 (1463^{+66}_{-68} pc; Bailer-Jones et al. 2021) is consistent with that of the SNR. Owing to the precision of *Gaia* DR3 (Gaia Collaboration 2016b, Gaia Collaboration 2023j), we have re-initiated our search for OB-runaway stars inside SNRs.

Previously, in Boubert et al. (2017), based on *Gaia* DR2 data, pre-SN companions inside the SNRs which are linked to a neutron star, and closer than d < 1−2 kpc, have been searched, and a few candidates have been proposed. We will present the spectra and discuss one of these candidates, BD+50 3188 inside SNR G089.0 + 04.7 in the next paper where we will share our findings on the SNRs between Galactic longitudes 53°−108°. Kochanek (2021) has also searched for runaway stars inside the SNRs again with known compact objects. They have confirmed that HD 37 424 is a solid example of a binary ejected runaway star.

In our search, first of all, we concentrate on all well-studied SNRs within a large distance range of 5 kpc, regardless of having a compact object. Secondly, we search for OB-type stars as they guarantee the young age and a low chance projection possibility. Additionally, we exclude the walk-away stars, again to avoid the chance projection.

In this paper, we report our findings of the search for OB-runaway stars inside 12 well-studied SNRs for Galactic longitudes 109°−206°, using the *Gaia* parallax, proper motion, and colour excess values as well as the spectral identification of 81 stars based on spectroscopy performed between 2013 and 2021. The possible OB-runaway stars are mentioned, the OB-runaway frequency is discussed, the SNR distance estimates are improved, the extinction towards them are determined, and possible progenitors are shown.

In Chapter 2, the selected sample of SNRs with or without NSs are introduced and the selection of OB-type star candidates are explained. In Chapter 3, the observations carried out and data analysis are explained in details. The results of the observations and candidate selection for each SNR are shared in Chapter 4 with the evaluation of the general picture.

2 THE SAMPLE AND THE METHOD

We performed the search for OB-runaway stars in 12 SNRs within 5 kpc from the Sun and observable from the Northern hemisphere. We expect that an OB-runaway candidate shows a consistency in position and the distance of the SNR. Therefore, we selected the SNRs that have been extensively studied in the literature. The SNRs in which we searched for OB-runaways are listed in Table 1. The SNR distance estimates are mainly based on the systematic velocity of the interacting clouds. However, the uncertainty is high and the interpretations are somewhat subjective. In this paper, we tried to estimate distances by a combination of different methods. We tried to detect massive stars and possible host open clusters for the SNRs as well as star-forming regions or young open clusters nearby, to have an idea of the progenitor origin. We also check an obvious interaction with molecular clouds and compare these distances with those derived from surface brightness–diameter (Σ–D) relation (Poveda & Woltjer 1968).

Some of the possible star-forming regions have not been detected before, or the distances to the known regions have been determined before the *Gaia* era. Thus, utilizing the high-quality *Gaia* DR3 astrometry, we estimated the distances to the star-forming regions near the SNR using the geometric distances (All' geometric distances'

Table 1. The SNRs in the sample. Column 1: Galactic coordinates, Column 2: Type of SNR [Shell type (S), Thermal Composite (TC), Plerion (P)], Column 3: Parallax interval for the runaway search, Column 4: Angular radius of search region, Column 5: Maximum extinction used in spectral type estimation, Column 6: The latest spectral type that we can detect for candidates for the given parallax and extinction values, Column 7: Existence of a compact remnant. References are in Section 4.

SNR	SNR Type	Parallax (mas)	Search Rad. (arcmin)	Max Av (mag)	Limit SpT	Comp. Rem.
G109.1 − 1.0 (CTB 109)	S	0.2–0.4	2.5	3	B8-B9	1E 2259 + 586
G111.7 − 2.1 (Cas A)	S	0.2–0.4	0.5	5	B3-B8	CXOU J232327.8 + 584842
G114.3 + 0.3	S	0.2–2.0	7.5	3	B8-B9	PSR B2334 + 61
G116.9 + 0.2 (CTB 1)	TC	0.2–1.0	3.0	3	B8-B9	–
G126.2 + 1.6	S	0.15–0.3	6.0	4	B4-B8	–
G127.1 + 0.5	S	0.3–1.0	4.0	4	B8-B9	–
G130.7 + 3.1 (SN 1181?)	P	0.2–0.5	0.75	4	B5-B9	PSR J0205 + 6449
G132.7 + 1.3 (HB 3)	TC	0.3–0.5	6.0	3	B9	–
G160.9 + 2.6 (HB 9)	TC	0.3–1.5	12.0	3	B9	–
G166.0 + 4.3 (VRO)	TC	0.15–0.5	5.0	3	B6-B9	–
G184.6 − 5.8 (Crab)	P	0.25–0.7	0.6	3	B9	PSR B0531 + 21
G189.1 + 3.0 (IC 443)	TC	0.3–1.0	4.0	4	B8-B9	CXOU J061705.3 + 222127

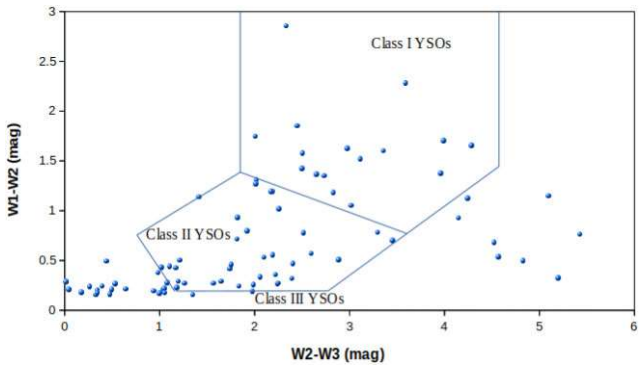

Figure 1. Classification of YSOs in the colour–colour diagram. The regions of Class III, II, and I YSOs around CTB 109 are shown.

throughout the paper are retrieved from Bailer-Jones et al. 2021) of young stellar objects (YSOs). To do that, we first had to find the YSOs.

YSOs are distinguished from main-sequence stars by their dense circumstellar material as well as their accretion disks, and outflows. The main observational evidence, necessary for confirming YSOs is the excess radiation in mid-infrared (MIR) due to the circumstellar material.

We have identified YSOs using the 3.4, 4.6, 12, and 22 μm (*W*1, *W*2, *W*3, and *W*4, respectively) band photometry of the Wide-field Infrared Survey Explorer (*WISE*; Wright et al. 2010). The values were retrieved from the *all 'WISE'* catalogue. To avoid spurious sources due to the nebulosity, we selected only the sources for which there are JHK_s band detections in the Two Micron All Sky Survey (2MASS) catalogue (Cutri et al. 2003, II/246) within 2 arcsec from the *WISE* position. To distinguish the YSOs from the other IR excess sources in colour–colour diagrams, we applied the selection criteria defined in Koenig & Leisawitz (2014). Besides the position of the YSO candidate in the *W*1–*W*2–*W*3 colour–colour diagram, an upper limit of 13 mag in the *W*1 band was applied. This worked well to distinguish the class II YSOs from the star-forming areas. The colour–colour diagram of the YSOs found within 20 arcmin from the geometrical centre of CTB 109 are shown in Fig. 1. The colour differences of the sources are given in Table C2.

We selected 12 SNRs at Galactic longitudes 109°−206°. We will report the SNRs at Galactic longitudes 34°−106° in another paper. Due to the high chance projection possibility, the SNRs that are close to the Galactic Centre are ignored. The SNRs studied in this paper are northern sky objects in a well-defined shape and well studied in the literature and are all probably within 5 kpc from the Sun (more or less high-quality *Gaia* parallax limit). They are mostly shell type and evolved. Crab Nebula and SNR G130.7 + 3.1 are the only two plerions. Five of them are thermal composites (mixed morphology (MMSNR)). Cas A, Crab, and G130.7 + 3.1 would be younger than one millennium (if G130.7 + 3.1 is related to the historical SN 1181).

Seven of the SNRs are linked to an NS (Table 1). Two of the five rotationally powered pulsars show characteristic ages very high compared to their kinematical ages (Table 2). One neutron star having a bright pulsar wind nebula (PWN) was thermally detected in X-rays, but no pulses were observed in any wavebands. Overall, the SNR sample represents the large variety of types and compact objects (Table 1).

The method followed in our work is a direct study of possible runaway stars inside SNRs as described in G05. Assuming that the massive binary mass ratio is greater than 1:4, we searched for OB-type runaway stars inside SNRs. The possible runaway stars with an effective temperature below 10 000 K are excluded.

Most of the OB-runaways have peculiar velocities lower than 80 km s^{-1} (Gies & Bolton 1986; Philp et al. 1996; Tetzlaff et al. 2011b). As the shock wave velocity of the SNRs is decelerated from roughly 10 000 km s^{-1} to several hundred km s^{-1}, it is expected that the runaway star cannot exceed one tenth of the angular radius (θ) of the related SNR. This value is somewhat relaxed to $\theta/6$ considering the uncertainties in the geometrical centres of the SNRs.

We choose the stars of which geometric distances are consistent with the distance of the related SNR. The parallax interval we set for each SNR can be seen in Table 1. The quality criteria for the parallax is $R > 5$ (measurement/error ratio).

The peculiar velocity of an OB-runaway star should be larger than $\geq$25 km s^{-1} in 3D and $\geq$17.6 km s^{-1} in 2D (Tetzlaff, Neuhäuser & Hohle 2011a). We obtained the *Gaia* proper motion for the stars, correct them for Galactic rotation and solar peculiar motion, and translate them into transverse velocities. If the transverse velocity is larger than 17.6 km s^{-1}, then the star is selected.

We also expect that the motion of the star in 2D should be pointing away from the geometrical centre of the SNR. As the geometrical

Table 2. The NSs of the SNRs in the sample are shown with their host SNRs and observational properties: period, period derivative, dipole magnetic field strength, and characteristic ages, respectively. References are in Section 4.

Name	P (s)	$\dot{P}$ (s s^{-1})	B (Gauss)	τ (yr)	Type
1E 2259 + 586	6.979	4.712×10^{-13}	5.80×10^{13}	235000	Magnetar
CXOU J232327.8 + 584842	1.061	–	–	–	CCO
PSR B2334 + 61	0.495	1.934×10^{-13}	9.91×10^{12}	40600	Radio PSR
PSR J0205 + 6449	0.066	1.938×10^{-13}	3.61×10^{12}	5370	X-ray Psr-PWN
PSR B0531 + 21	0.033	4.210×10^{-13}	3.79×10^{12}	1260	Psr-PWN
CXOU J061705.3 + 222127	–	–	–	–	CCO?-PWN

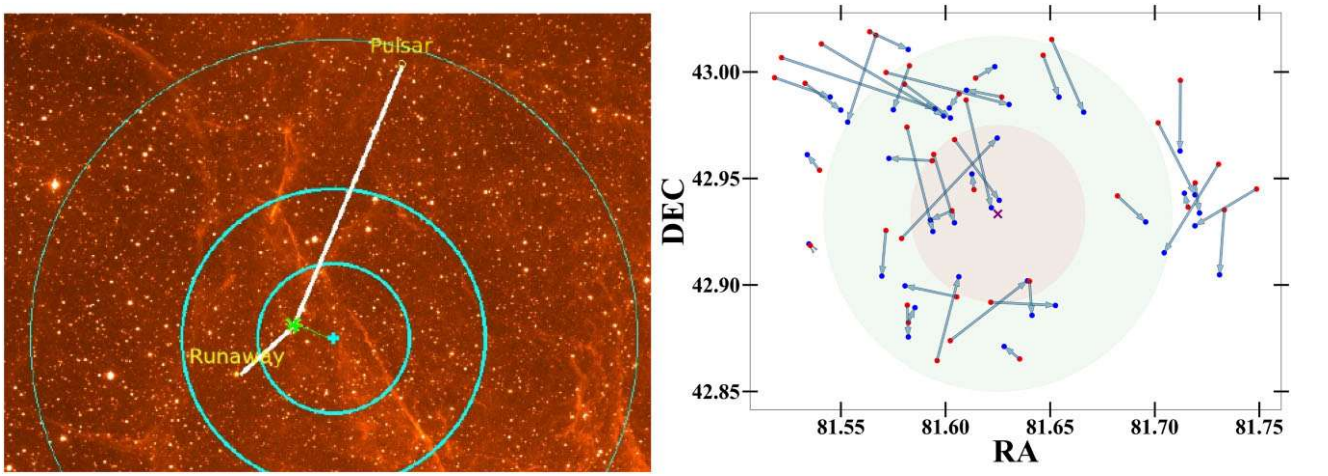

Figure 2. *Left*: H α image of the central region of SNR S 147 taken with Schmidt–Telescope–Kamera (STK) at the University Observatory, Jena. The filaments belong to the SNR. A candidate must have a transverse velocity higher than 17.6 km s^{-1} and must be moving away from the geometrical centre of the SNR like in the case of HD 37424 (Dinçel et al. 2015). The proper motion of the runaway star is traced back for 30 kyr (white lines) and found to be at the same position with the pulsar near the geometrical centre 30 kyr ago. The larger cyan circle represents the search region, while smaller cyan circle is the error circle of the geometrical centre. *Right*: 60 kyr traced back proper motion vectors of the stars having a higher transverse velocity of 17.6 km s^{-1} in the central region of the SNR G166.0 + 4.3. The larger circle is the search region and the smaller is the geometrical centre error circle. The star number 2 satisfied all criteria and is selected as a candidate.

centre cannot be accurately specified, we defined a circle with a radius of half the search region radius, which is one-twelfth of the SNR radius, for the error circle of the geometrical centre (Fig. 2). In the case of elliptic shaped SNRs, the larger radii were chosen not to underestimate the uncertainty. Then, the proper motion of the stars with consistent parallax values and transverse velocity larger than 17.6 km s^{-1} were traced back in time up to 60 kyr (assumed to be the maximum age of the remnants in the sample). Although the observable lifetime of the SNRs are thought to be 100 kyr, the age of the SNR S 147, which is one of the largest SNRs in the literature (78 pc), was found to be 30 kyr (Dinçel et al. 2015). As Sedov solution set an upper limit to the age, the real ages of the SNRs might be smaller. Therefore, we set the maximum flight time of a runaway star as 60 kyr, twice the age of S 147. The stars, for which the proper motion vector can be traced back to intersect the error circle around the geometrical centre within 60 kyr, are then selected for further investigation.

Finally, these sources have been checked if they are hot stars. There is no spectroscopic data for the vast majority of the candidates; therefore, the temperature of candidates is estimated through photometry. Using *Gaia* $G_{BP}GG_{RP}$ and 2MASS JHK_s photometry, the A_V values are calculated for temperatures between $\log T_{\rm eff}[{\rm K}] = 3.6$–4.5 divided to 131 steps, with each colour difference, i.e. $G_{BP} - G_{RP}$, $J - K_s$, $G_{BP} - J$, etc. The intrinsic colour differences, i.e. $(G_{BP} - G_{RP})_0$ for an isochrone with $\tau = 10$ Myr and solar metallicity, were retrieved from 'CMD 3.0'[1] using PARSEC 1.2S evolutionary tracks (Chen et al. 2015) with bolometric corrections from Girardi et al. (2008) and the extinction curve from Cardelli, Clayton & Mathis (1989) and O'Donnell (1994) with an extinction law $R = 3.1$. The standard deviation σ of the A_V values calculated from each colour pairs by the relation,

$$A_V = \frac{(\lambda_1 - \lambda_2) - (\lambda_1 - \lambda_2)_0}{A_{\lambda_1}/A_V - A_{\lambda_2}/A_V}, \quad (1)$$

is supposed to be the smallest at the true effective temperature of the star. However, the uncertainties of spectral type estimation from photometry are high. Therefore, to avoid underestimation of the errors, we applied an average cut. The possible temperature of the star is an interval between the values where the temperature curve intersects the average σ value (Fig. 3). If the maximum temperature is larger than $T_{\rm eff} = 10\,000$ K, then the star is considered as an OB-runaway candidate.

Due to the large uncertainties, some later-type stars, i.e. A-type stars may not be eliminated by pure temperature estimation. The A_V values of the stars satisfying this condition are therefore compared with the values of the spectroscopically observed stars (see Section 4). An interval of extinction values towards the SNR is generated

[1](http://stev.oapd.inaf.it/cmd)

Table 3. List of observations. The dates of observations, observatories, used spectrographs, their resolving power R, grisms used, and the wavelength ranges are given.

Date	Observatory	Telescope	Instrument	Res.	Grism	Wavelength range (Å)
2012 Sep 12–13	TUG	RTT-150	TFOSC	1300	G14	3270–6120
2013 Jan 29	Calar Alto	2.2-m	CAFOS	550	B-200	3850–5000
2013 Feb 11–12	TUG	RTT-150	TFOSC	1300	G14	3270–6120
2013 Jul 18–19	Calar Alto	2.2-m	CAFOS	550	B-200	3850–5000
2013 Aug 09–10	TUG	RTT-150	TFOSC	1300	G14	3270–6120
2013 Jul 30	U Jena	90-cm Schmidt	FLECHAS	9200	Échelle	3900–8100
2014 Jan 12–13	Calar Alto	2.2-m	CAFOS	550	B-200	3850–5000
2015 Jan 07–08	Calar Alto	2.2-m	CAFOS	550	B-200	3850–5000
2015 Feb 22	U Jena	90-cm Schmidt	FLECHAS	9200	Échelle	3900–8100
2015 Mar 16–17	U Jena	90-cm Schmidt	FLECHAS	9200	Échelle	3900–8100
2015 Oct 19	TUG	RTT-150	TFOSC	1300	G14	3270–6120
2015 Jan 09	SAO	FLWO 1.5-m	TRES	44 000	Échelle	3800–9100
2021 Dec 29	NAOJ	Subaru	FOCAS	3000	VPH-450	3800–5250

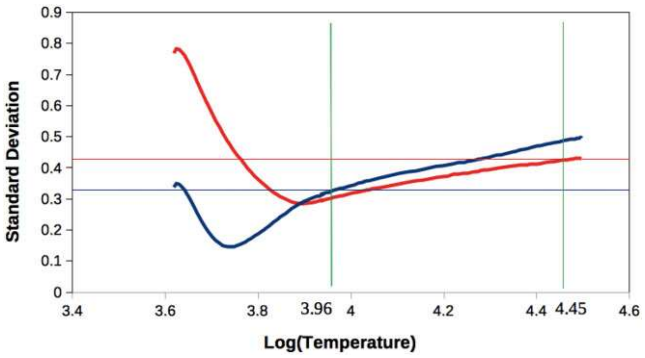

Figure 3. Estimation of effective temperature. An example of a possible cool (blue) and possible hot candidate (red) determined by the maximum temperature value after the mean value cut.

by using the stars of which the spectra had been taken previously. If the minimum A_V value of the star is comparable with the extinction towards the SNR, then the star is finally a candidate.

The spectral-type estimation from photometric catalogues are not used, as they provide discrete values instead of a range of values. For example, in *Starhorse 2* catalogue (Anders et al. 2021), 18 out of 48 OB-type stars that we confirmed by spectroscopy are found to have an effective temperature of $T_{\rm eff} < 10\,000$ K, 12 of which has a $T_{\rm eff} < 9000$ K.

To summarize, a main-sequence OB-type star within an SNR with a transverse velocity $\geq$17.6 km s^{-1} and 2D motion pointing away from the geometrical centre of its SNR is considered a good candidate, so that we will consider it further.

The spectrum of the candidates are taken to confirm their spectral type and measure the radial velocities.

3 OBSERVATION AND DATA REDUCTION

To confirm the OB-runaway nature of the candidates, their spectra were obtained and studied.

We selected the first runaway star candidates already before the *Gaia* mission based on UCAC4-2MASS data (as in Dinçel et al. 2015), so that some follow-up observations had already been performed before the *Gaia* data became available. Then, with the *Gaia* DR3 data, we iterated the selection – many candidates were omitted, others were added (and observed). The omitted candidates were used to determine the extinction towards the SNRs which is vitally important to find OB-type candidates through photometry.

Between 2013 and 2014, low-resolution spectra of 173 stars were taken throughout the candidate selection before *Gaia* era with Calar Alto Faint Object Spectrograph (CAFOS)[2] mounted on 2.2 m telescope at Calar Alto Observatory in Almeria, and with TUG Faint Object Spectrograph and Camera (TFOSC) mounted on RTT-150 at TÜBİTAK National Space Observatory (TUG)[3] in Antalya. Eighty of these spectra were used in this work to determine the extinction towards the central region of the SNRs. High-resolution spectra of 19 bright targets were taken with the Fibre Linked Échelle Astronomical Spectrograph (FLECHAS; Mugrauer, Avila & Guirao 2014) on the 90 cm Schmidt telescope at the University Observatory Jena and Tillinghast Reflector Échelle Spectrograph (TRES) on the 1.5-m Tillinghast telescope at the Smithsonian Astrophysical Fred L. Whipple Observatory on Mt. Hopkins in Arizona to measure the radial velocity of the stars and the accelerated lines of the interstellar medium (ISM). These stars are not runaway candidates any more, yet the accelerated ISM lines due to the SNR expansion provides us valuable information on the SNRs. Low-resolution spectra of two candidates selected by using *Gaia* DR3 data and three other stars for extinction measurements were taken with the Faint Object Camera and Spectrograph (FOCAS)[4] installed on the Cassegrain focus of 8-m Subaru Telescope at the National Astronomical Observatory of Japan in Hawaii. The information on the instruments and the list of observations are given in Table 3.

The purpose of observations is divided into three: (i) the low-resolution spectra of candidates before *Gaia* DR3, which are used for extinction determination towards the SNRs, the high-resolution observations of bright neighbouring stars to study the extinction to the SNRs and the radial velocity of ISM features, and (iii) low-resolution spectra of *Gaia* DR3 candidates to determine their spectral types.

In this chapter, the observations, data reduction, and analyses are explained.

[2]https://www.caha.es/alises/cafos/cafos.html, Accessed on 2016 November 01.
[3]http://tug.tubitak.gov.tr/tr/teleskoplar/tfosc. Accessed on 2016 November 06.
[4]'https://www.naoj.org/Observing/Instruments/FOCAS/index.html' Accessed on 2021 March 02.

Table 4. Results of Fourier cross correlation of CAFOS spectra of HD 278115 and TYC 3572-00017-1 with their own TFOSC spectra (last column) and with standard stars of various spectral types.

Star	F0V	A0V	B5V	B3V	B2V	B1V	O9V	TFOSC
TYC 0017	0.844	0.876	0.921	0.933	0.955	0.933	0.906	0.963
HD 278115	0.815	0.872	0.888	0.891	0.925	0.937	0.927	0.973

3.1 Observations

For spectral-type identification, the wavelength range chosen in this work is λ 3850–5000 Å following the Morgan–Keenan standards (Morgan, Keenan & Kellman 1943). Low-resolution spectra were taken throughout the same procedure. The CCDs of all three instruments were cooled down to and fixed to −100°C to avoid count variations due to the temperature. So, no dark frames were observed. Instead, ten bias frames were taken and the overscan region of the science frames, which is kept dark along the integration was used. Five halogen lamp spectra for flat fielding and five arcs for wavelength calibration were taken. The arc lamps observed for CAFOS, TUG, and FOCAS were Hg-He-Rb, He, and Th-Ar, respectively.

FLECHAS and TRES providing a resolving power of $R \sim 9000$ and $R \sim 44\,000$, respectively, were adequate for radial velocity measurements. The limiting m_v for both instruments are 11–12 mag. The arcs (Th-Ar lamp) and flats (Tungsten lamp) of the high-resolution spectra were taken immediately before the science exposure to ensure the radial velocity accuracy. Unlike others, the CCD of FLECHAS were cooled down to −25 and −35 °C. Therefore, a set of dark frames were taken for each integration time of the science exposures.

3.2 Data reduction

The reduction of TRES data were done by using the TRES IDL pipeline. The other data obtained were reduced in the IRAF environment (Tody 1986).

The data processing for TFOSC, CAFOS, and FOCAS instruments are the same. Ten bias frames were combined to have an average background and were subtracted from the science, flat, and arc frames, which were also overscan stripped through *x*-axis by their own dark region. Afterwards, multiple science frames were combined with average sigma clipping rejection to remove cosmics. Five flats were combined to average, and the science frames were divided by it. The bias-dark correction and flat fielding were performed through the IRAF task *ccdproc*. Five arcs were also combined to average. The arc and science spectra were then be extracted using the task *apall*. The science spectra were sky background subtracted during extraction. Each arc was extracted by tracing the corresponding science spectrum. The emission lines of the extracted arc spectrum were identified following the line identification maps made particularly for the instruments. The dispersion solution was created by the task *ident*. After all science spectra were wavelength calibrated, they were normalized using the task *continuum*.

FLECHAS images were subtracted by the dark frames of which exposure time is the same as that of the corresponding science or calibration frame. Hence, the dark current was removed. After dark removal, the flats of FLECHAS, which were taken for each target frame, were first extracted tracing each échelle apertures of the science and then used for flat fielding of the correspondent spectrum. The rest of the data reduction of FLECHAS data follow the steps mentioned above.

3.3 Spectral-type determination

For the spectral-type identification of the CAFOS and TFOSC data, the spectra of Morgan–Keenan standard stars observed at Dark Sky Observatory with a dispersion of 1.8 Å pixel^{-1} were retrieved from the web page.[5] The standard spectra were smoothed via boxcar by values 7 and 3, respectively, due to its higher dispersion. Each spectrum was cross-correlated with all of the standard spectra from B to K type by using the IRAF task *fxcor* (Fig. A1). The spectral type, yielding the largest correlation height was assigned (Fig. A1). The error in spectral type was determined as ±1, as the correlation height is significantly smaller at further types. Beyond 1 digit error, we expected that the correlation height would be 0.04 smaller than the maximum value. This 0.04 limit was found by cross-correlating the CAFOS spectra of two stars with their own TFOSC spectra. Although the stars are the same, the correlation height was not exactly 1.0, but ≤0.04 smaller (Table 4). Therefore, this difference set the error. However, for B2-type stars, the correlation height with B5 was found also high (Table 4). On the other hand, B5-type stars show a significantly stronger Mg II (4481 Å), line, so this can be easily distinguished by visual inspection. Such fine tunes were made using the relative intensities (w.r.t. H) of 4686 Å He II for very hot stars, 3933 Å Ca II–K, *G* band at ∼4300 Å, and 4227 Å Ca II for late-type stars. In addition, with CAFOS spectra the luminosity class V may not be distinguished from the luminosity class III due to its low-spectral resolution.

4 RESULTS

Based on the methods described in Section 2, an OB-runaway star is searched inside the SNRs as a pre-SN binary companion to the progenitor. To show the reliability of the results, the distance and the extinction to the SNRs are widely discussed. The extinction towards the central regions of the SNRs are measured using the spectroscopic observations of the stars close to the central region.

Two good runaway star candidates were identified. Low-resolution Subaru/FOCAS spectra were taken. One star could be rejected as OB-runaway star, while the spectral type of the other could not be determined due to the low signal to noise.

We list distances, ages, and extinctions for the SNRs studied, as determined by us in Table 6.

4.1 G109.1–1.0 (CTB 109)

CTB 109 is a shell-type SNR, having a relatively small angular diameter of 27 arcmin (Fig. 4). It hosts a magnetar, AXP1E2259 + 586, which is close to the centre of CTB109. The position coincidence is evidence for their association, which is also supported by the direction of the proper motion, pointing away from the centre, to the west. X-ray outbursts yield an energy release of 5×10^{36} erg s^{-1} (Kaspi et al. 2003). The magnetar has a relatively low surface dipole magnetic field strength, $B_{\rm dip} = 5.9 \times 10^{13}$ G. Its period and period

[5] ned.ipac.caltech.edu/level5/Gray/Gray1.html.

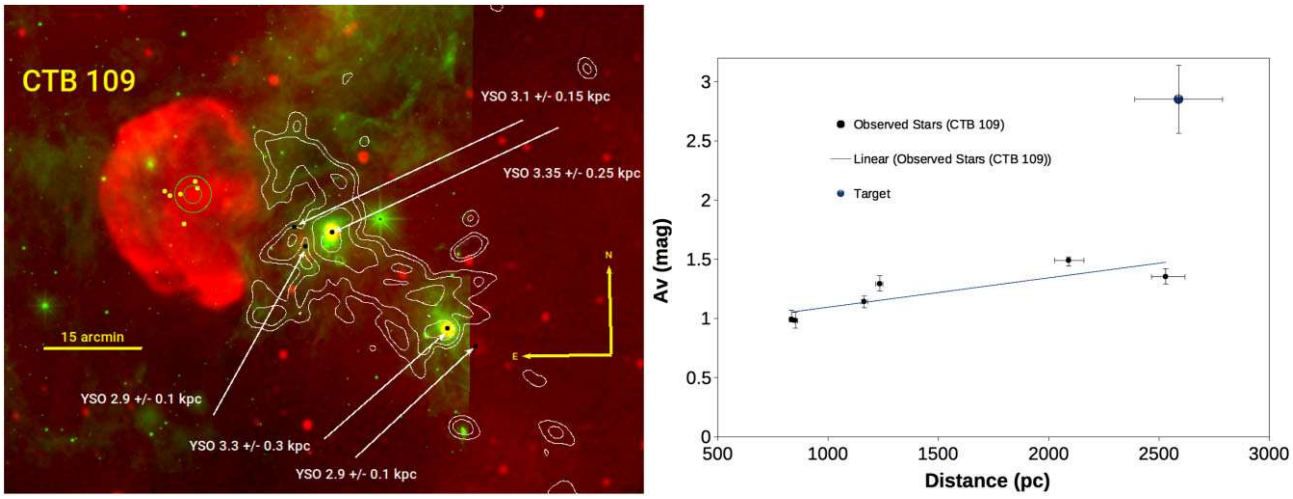

Figure 4. *Left*: Colour composite image of SNR CTB 109 and its surrounding. The 1420 MHz image of the SNR (red) is retrieved from Canadian Galactic Plane Survey (CGPS), and green is the *W3* band image of *WISE* Survey, retrieved from *Skyview*. White contours overlaid is the CO map at −51 km s^{-1} taken from CGPS. Black dots show the massive YSOs, mostly transition disc objects, which belong to the star formation regions inside the giant molecular cloud. Their rough geometric distances are given. The two green circles (big and small), in the middle of the SNR, are the OB-runaway search region and the geometrical centre region, respectively. The yellow dots are the stars we have taken the spectra and used for the determination of A_V values. *Right*: Radial distribution of extinction towards the central region of SNR CTB 109. One of the target stars that succeeded the kinematical criteria, has considerably higher minimum A_V value, indicating that it does not have a high surface temperature.

derivative ($P = 6.98$ s, $\dot{P} = 4.837 \times 10^{-13}$ ss^{-1}; Dib & Kaspi 2014) yield a characteristic age of 230 kyr which is very high compared to the age of the remnant (15−40 kyr), and a low-energy dissipation of $E \approx 10^{31}$ erg s^{-1}.

CTB 109 is interacting with a giant molecular cloud (GMC) in the west, which caused the vanishing of the shock front in this direction, so the shell has a semicircular shape (Sasaki et al. 2006). The systematic velocity of the GMC varies between −48 and −56 km s^{-1}(Tatematsu et al. 1990; Kothes, Uyaniker & Yar 2002). The shape of the cloud is compatible with an SNR morphology at −51 km s^{-1} (Fig. 4). Although this velocity corresponds to a kinematic distance of 5.0 ± 0.5 kpc, 2.8–4.0 kpc is suggested considering the velocity dispersion in Perseus arm due to the density wave shock (Foster & MacWilliams 2006; Tian, Leahy & Li 2010). The H II regions Sh 2−152 and Sh 2−153 are located in the south east of the SNR at a distance of ∼3.21 ± 0.21 kpc (Ramírez Alegría et al. 2011). These star-forming regions are thought to be a part of the GMC in interaction with CTB 109. Hence, the suggested distance to the SNR is 3.2 ± 0.2 kpc (Kothes & Foster 2012).

Based on *XMM–Newton* and *Chandra* observations, the X-ray emitting plasma was found to be at a temperature of $k\,T = 0.25 \pm 0.03$ keV. This translates to a blast wave velocity of $v_{\rm bw} = 460 \pm 30$ km s^{-1}. From Sedov solution, the age was derived as 14000 ± 2000 yr. This is far below the characteristic age of the magnetar, which is $\tau = 230$ kyr. The SN ejecta show that the SNR has a core-collapse origin (Sasaki et al. 2013). The spatial variation of $N_{\rm H}$ is high; $(0.5-1.5) \times 10^{22}$ cm^{-2} ($A_{\rm V} = 2-7$ mag), consistent with the values found for the magnetar (Zhu et al. 2008).

Based on the geometric distances, the massive young stars and YSOs lying in the south-west of the SNR, in the H II regions (Fig. 4) are at a weighted mean distance of 3106^{+193}_{-156} pc (Table C2). Considering also previous estimations, we suggest a distance of 3.1 ± 0.15 kpc for the SNR.

Our extinction measurement does not extend to the possible distance of the SNR (Fig. 4). The foreground stars show a low value of extinction, i.e. $A_V \sim 1.3$ mag at 2.5 kpc. Extrapolation yields a value of 1.6 mag at 3.0 kpc. However, owing to the GMC, the extinction has a large spatial variation and can increase up to 7 mag. Nevertheless, CO images show that the central region seems to be free from the obscuration of the GMC. Therefore, we searched for OB-runaway star up to an extinction of $A_V = 4.0$ mag and a distance of $d = 4.0$ kpc. There is no OB-runaway star related to the CTB 109 and its magnetar. We expected to find one as the SNR is in interaction with star-forming regions, implying a massive progenitor. Although it was mentioned that it was a crude estimation, the ejected mass of the SNR is >20 M$_\odot$ (Sasaki et al. 2013). Such a high ejected mass might be possible by merging of two massive star. Increased spin angular momentum of the core might have initiated the dynamo action (Duncan & Thompson 1992), which resulted in a magnetar.

4.2 G111.7 − 2.1 (Cas A)

Cas A is a very young SNR with a bright radio shell (Anderson et al. 1991). The age was measured from the optical expansion of the dense knots and found as 353 ± 27 yr (Fesen et al. 2006). Probably due to the high reddening, the explosion could not be seen by any observer. An extinction of $A_{\rm V} = 5-6$ mag is suggested (Hurford & Fesen 1996). However, the $N_{\rm H}$ values measured from the X–ray observations corresponds to $A_{\rm V} = 8$–9 mag (Hughes et al. 2000). The estimated distance towards the SNR is $3.4^{+0.3}_{-0.1}$ kpc (Reed et al. 1995).

Cas A has a core-collapse origin, which resulted in a type IIb SN (Rest et al. 2011). It is a typical O-rich SNR hosting a neutron star, right in the geometrical centre, observable in X-rays (Lazendic et al. 2006). Although the thermal radiation can be observed, no pulsations were detected so far. Furthermore, non-thermal emission could be a sign of a PWN, but it is not detected. Thus, the NS is thought to be a central compact object (CCO) with a very slow spin and low $B_{\rm dip}$ (Pavlov & Luna 2009). Given the properties, the Cas A progenitor must be a massive star. A pre-SN binary companion inside Cas A has already been searched, but could not be found (Kochanek 2018).

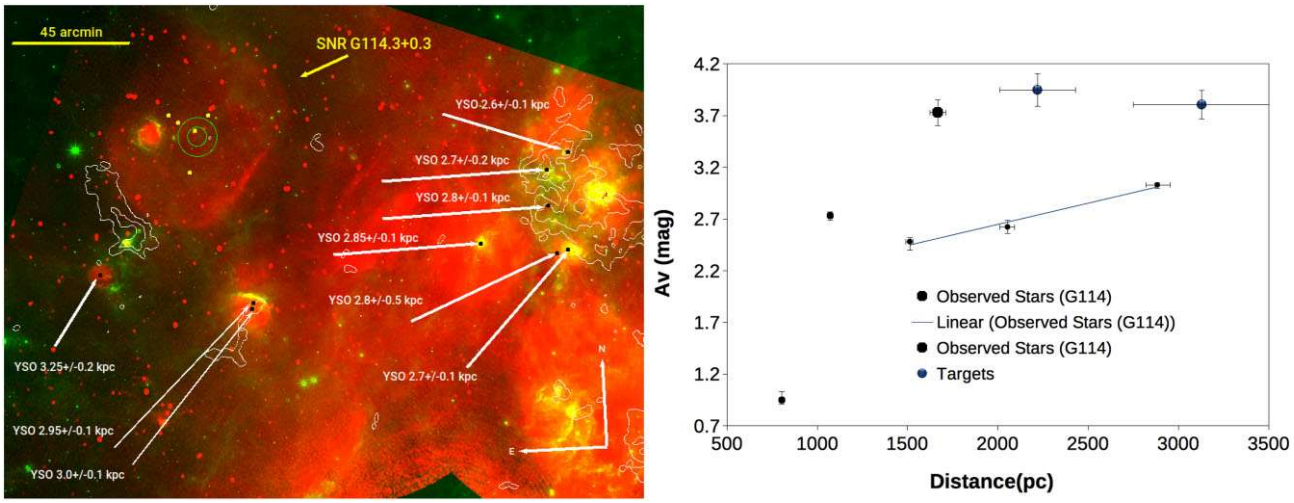

Figure 5. *Left*: Colour composite image of SNR G114.3 + 0.3 and its surrounding. Red represents the 1420 MHz image from CGPS, while green is the *W3*-band image of the *WISE* Survey, retrieved from *Skyview*. White contours overlaid is the CO map at −50 km s^{-1}, taken from CGPS. Black dots show the massive YSOs, mostly transition disc objects, which belong to the star formation regions inside the GMC. The rough geometric distances are given. The two green circles (big and small), in the middle of the SNR are the OB-runaway search region and the geometrical centre region. The yellow dots are the stars of which we have taken the spectra and which were used for the determination of A_V values. *Right*: Radial distribution of extinction towards the central region of CTB 109. Some target stars exhibit very high minimum A_V value, so they fail to be a candidate.

We did not find any OB-runaway candidate in the central region of Cas A up to a distance of 4 kpc and a maximum extinction of 5 mag.

4.3 G114.3 + 0.3

G114.3 + 0.3 is a shell type SNR with an angular size of about 90 arcmin × 55 arcmin (Green 2009). The radio shell has a circular shape in the south and mostly diffuse in the north (Fig. 5). The shell is diffuse and faint in optical bands. The velocity of the shocked filaments is ∼100 km s^{-1}. No X-ray emission was detected from the SNR. G114.3 + 0.3 is considered to be an evolved SNR in the radiative phase (Mavromatakis, Boumis & Paleologou 2002).

The compact remnant is PSR B2334 + 61, a thermal X-ray pulsar with radio pulsations at a period of 495 ms. The period derivative is $\dot{P} = 1.93 \times 10^{-13}$ s s^{-1}, yielding a characteristic age of $\tau = 40600$ yr (Yuan et al. 2010). PSR B2334 + 61 has an ordinary dipole magnetic field strength of $B_{\rm dip} = 9.9 \times 10^{12}$ G. A dispersion measure (DM) of 58.38 ± 0.09 pc cm^{-3} for the pulsar yields a distance of 3.15 ± 0.5 kpc (Mitra et al. 2003), based on the Galactic electron distribution (Cordes & Lazio 2002). The distance is, however, 2.5 ± 0.5 kpc, using the previous electron distribution from Taylor & Cordes (1993) and 2079 pc based on the model by Yao (Yao, Manchester & Wang 2017). The X-ray spectrum from *XMM–Newton* observations suggests a hydrogen atmosphere at a temperature of $T = 0.65 \times 10^6$ K with $N_{\rm H} = 3.3 \times 10^{21}$ cm^{-2} (McGowan et al. 2006). The $N_{\rm H}$ corresponds to an optical extinction of $A_{\rm V} = 1.5$ mag.

The H I clouds, which might be related to the SNR was found at velocities of −35 and −45 km s^{-1} (Reich & Braunsfurth 1981). This corresponds to distances of 3.2 and 4.2 kpc, respectively. Another H I cloud at −6.5 km s^{-1}, which translates to 550 pc, was proposed to be related to the SNR. Based on this value, a distance of 700 pc was suggested (Yar-Uyaniker, Uyaniker & Kothes 2004). On the other hand, the Σ–D diagram suggests a distance of 2.94 kpc (Guseinov et al. 2003). CTB 1, G116.5 + 1.1, and G114.3 + 0.3 were proposed to be located in a giant H I bubble of 280 pc diameter (Fich 1986). But, a recent work excludes G114.3 + 0.3 from the super bubble GS 118 + 01 − 44 (Suad et al. 2016).

Another indicator for the distance is the H II region Sh 2 − 165. Based on the polarization studies at 2.7 GHz, it was found that the H II region does not apply any Faraday rotation on the polarized emission of the SNR. Thus, the SNR should be located in the foreground to Sh 2 − 165 (Reich & Braunsfurth 1981). A distance of 1.96 ± 0.39 kpc was suggested for Sh 2 − 165 by Foster & Brunt (2015).

The geometric distance of BD + 61 2494 (B0V; Georgelin, Georgelin & Roux 1973) the ionizing source of the region, is $d = 1735^{+41}_{-47}$ pc. Through our spectroscopic observations, we found two B-type stars, *Gaia* DR3 2 015 537 687 127 368 832 (B2) and *Gaia* DR3 2 015 567 541 434 498 304 (B6), which are at 1513^{+19}_{-23} and 2883^{+70}_{-64} pc, respectively. We also derived a mean distance to the star-forming regions around the SNR, and obtained $d = 2856^{+185}_{-138}$ pc. Considering the distance to the pulsar and the low surface brightness of the SNR, a distance of $d = 2.85 \pm 0.35$ kpc is plausible. On the other hand, if we cannot exclude the fact that Sh 2 − 165 is a background source due to the lack of Faraday rotation, together with the early B-type star we found at 1.5 kpc, a distance of $d = 1.65 \pm 0.20$ kpc is also possible. Therefore, we suggest two possible distances for SNR G114.3 + 0.3, which are $d = 2.85 \pm 0.35$ and $d = 1.65 \pm 0.20$ kpc.

Taking the angular radius $R_\theta = 45$ arcmin, the shock radius of the SNR is 9.1 pc at 0.7 kpc, 21.6 pc at 1.65 kpc, and 37.3 pc at 2.85 kpc. At 2.85 kpc, the SNR is considered to be in radiative phase. Following McKee & Ostriker (1977), the age of the SNR is 22 700 yr for $E_0 = 10^{51}$ erg and $n_0 = 1$ cm^{-3}. The extinction increases steeply from 700 to 1000 pc. The trend line looks flatter between 1500 to 3000 pc. At 2.9 kpc, $A_V = 3.0$ mag. There is no OB-runaway star up to a distance of $d = 4$ kpc.

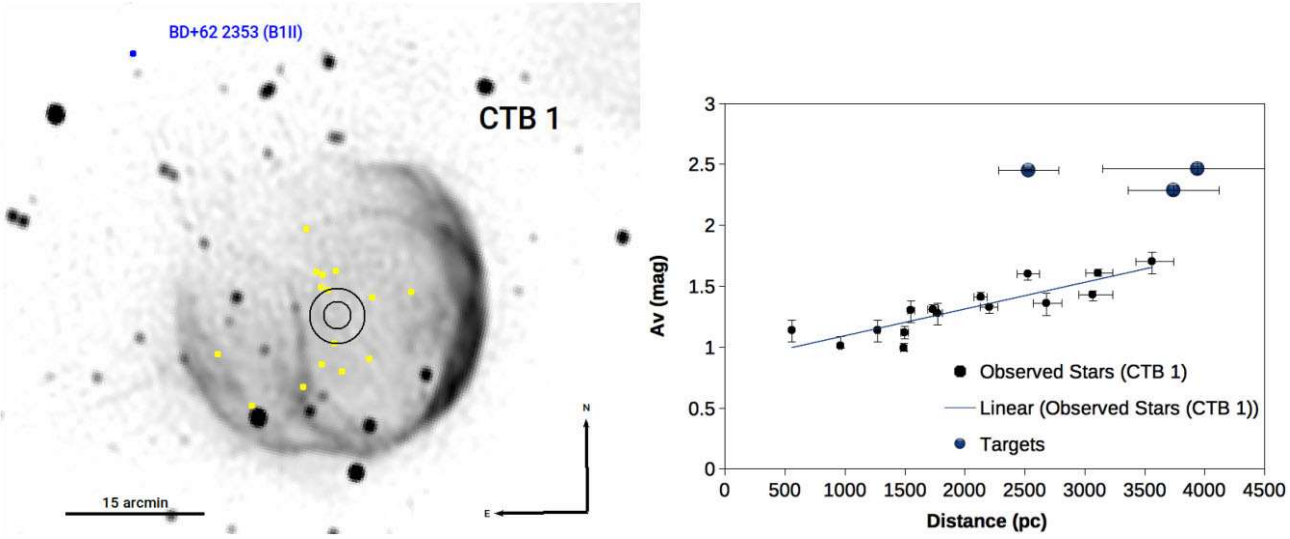

Figure 6. *Left*: 1420 MHz image of CTB 1 from CGPS. The two green circles (big and small), in the middle of the SNR are the OB-runaway search region and the geometrical centre region. The yellow dots are the stars of which we have taken spectra and which were used for the determination of A_V values. The cyan dot is the evolved massive star, which might have a gennetic connection with the progenitor. *Right*: Radial distribution of extinction towards the central region of CTB 1. Three of the targets have considerably higher minimum A_V values. They are most probably late-type stars.

4.4 G116.9 + 0.2 (CTB 1)

CTB 1 is a shell-type MMSNR with a diameter of about 34 arcmin (Green 2009). The morphology in the H α band is mostly spherical symmetric except for a breakout region in the northeast (Fig. 6). The SNR is centrally filled in X-rays. The X-ray emission also extends along the breakout region. Considering a filament density of 10 cm^{-3}, and an average velocity of the shocked filaments of $\sim$100 km s^{-1}, the age and the explosion energy was calculated as τ =16 kyr and $E_0 = 1.0 \times 10^{50}$ erg at 3.0 kpc (Fesen et al. 1997b). For 4.5 kpc, the initial explosion energy is $E_0 = 3.5 \times 10^{50}$ erg.

Based on *Chandra* observations, the temperature of the expanding plasma is 0.2 $\pm$ 0.02 keV. This translates to an expansion velocity of 410 $\pm$ 70 km s^{-1}. By the Sedov or evaporating cloud models, the age was found as 13000 $\pm$ 1500 yr for 3.0 kpc distance. The suggested explosion energy is even lower, $E_0 = (3.4 \pm 1.2) \times 10^{49}$ erg from the Sedov model and $E_0 = (1.5 \pm 0.7) \times 10^{50}$ erg from the evaporating clouds model (Lazendic & Slane 2006). The X-ray spectrum of CTB 1 is rich in O and Mg, indicating a core-collapse origin. The predicted progenitor mass is 13$-$15 M$_\odot$ (Pannuti et al. 2010).

The systematic velocity derived from H I measurements vary between $-$27 and $-$33 km s^{-1}. Together with the interpretations of the surroundings, the suggested distance is 2.4 $\pm$ 0.8 kpc (Landecker, Roger & Dewdney 1982; Hailey & Craig 1994; Yar-Uyaniker et al. 2004). Σ–D diagram suggests a higher value of 4.5 kpc (Guseinov et al. 2003). If 3.0 kpc is adopted, then the SNR is either expanding in a very low density medium or the initial explosion energy is very low. A_V was found as 1.64 mag (Fesen, Blair & Kirshner 1985). However, larger values were measured (Fesen et al. 1997b): 2.2–3.1 mag. The N_H measured by fitting the X-ray spectrum was (4.0$-$6.0) $\times$ 10^{21} cm^{-2} (Pannuti et al. 2010). Even higher N_H values, up to 8 $\times$ 10^{21} cm^{-2}, were suggested again from X-ray spectra (Lazendic & Slane 2006).

Two nearby OB associations, listed in Ward, Kruijssen & Rix (2020) with ID numbers 89 and 4, are at 3.1 and 3.6 kpc. The SNR has a breakout region, which is clearly defined in optical and X-ray observations. It resides in the south-western corner of a giant H I bubble with a systematic velocity of $-$44 to $-$50 km s^{-1} (Suad et al. 2016). These velocities imply a distance of 2.5–3.2 kpc, like in the cases of CTB 109 and G114.3 + 0.3. BD + 62 2353 is the possible generator of the bubble that CTB 1 is expanding into. The parallax measurement towards the star is not very accurate ($R \sim 5$), though the geometric distance is 4559 $^{+647}_{-593}$ pc. Another star, which might be responsible for the cavity is LS I + 62 63. Its spectral type is O9.5V. The geometric distance, which is precisely measured is 3190 $^{+139}_{-140}$ pc. There is also a number of massive stars near the SNR are at $\sim$3.1 kpc. A proper parallax measurement of BD + 62 2353 may reveal the distance to the SNR. Here, we can suggest a distance of $d = 3.2^{+1.3}_{-0.2}$ kpc.

The extinction seems to increase rapidly up to 1 mag at $\sim$0.5 kpc. After 0.5 kpc, the slope of the trend line is low (Fig. 6). The overall extinction is low (1.7 mag at 3.5 kpc).

We searched for OB-runaway stars for the parallax interval 0.2–1.0 mas with a maximum extinction of $A_V = 2.5$ mag. No OB-runaway star candidate was found.

4.5 G126.2 + 1.6

G126.2 + 1.6 is an SNR with a poorly defined shell, partially showing filamentary emission (Fig. 7). The angular diameter is about 70 arcmin (Green 2009). The O III/ H β ratio gives a shock velocity of $\sim$120 km s^{-1} (Boumis et al. 2005). The V_{LSR} of the H I related to the clouds vary between $-$33 and $-$55 km s^{-1}. Hence, the estimated distances show large variation; 2.0–5.6 kpc (Joncas, Roger & Dewdney 1989; Tian & Leahy 2006). For 5.0 kpc, the physical diameter of the SNR is about 128 pc. The Σ–D diagram yields a lower value of 2.88 kpc (Guseinov et al. 2003). The A_V towards the SNR is suggested as $\sim$1.4 mag (Blair et al. 1980).

TYC 4038-1657-1 is an A0Ib type star (Hardorp et al. 1959), which is only about 50 arcsec separated from the geometrical centre (Fig. 7). The geometric distance of the star is 4379$^{+298}_{-274}$ pc.

We also found two B-type stars near the centre, *Gaia* DR3 512 801 198 023 929 600 (B1) at 4624$^{+296}_{-279}$ pc and *Gaia* DR3

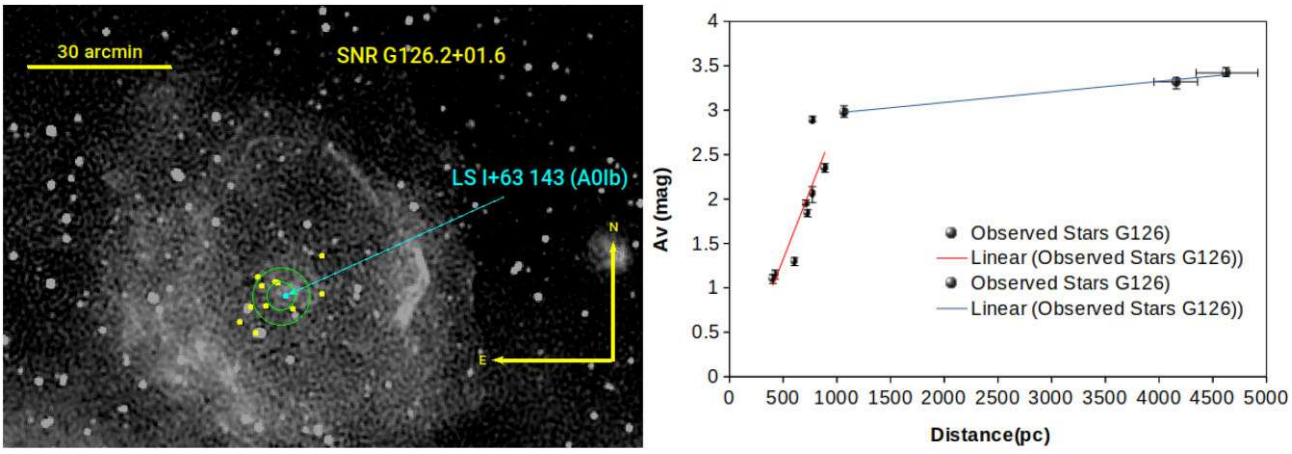

Figure 7. *Left*: 1420 MHz image of SNR G126.2 + 1.6 from CGPS. The two green circles (big and small), in the middle of the SNR are the OB-runaway search region and the geometrical centre region. The yellow dots are the stars of which we have taken spectra and which were used for the determination of the A_V values. The cyan dot is the evolved massive star that might have a genetic connection with the progenitor. *Right*: Radial distribution of extinction towards the central region of SNR G126.2 + 1.6. The steep increase of extinction towards ∼1 kpc is clearly visible in this plot.

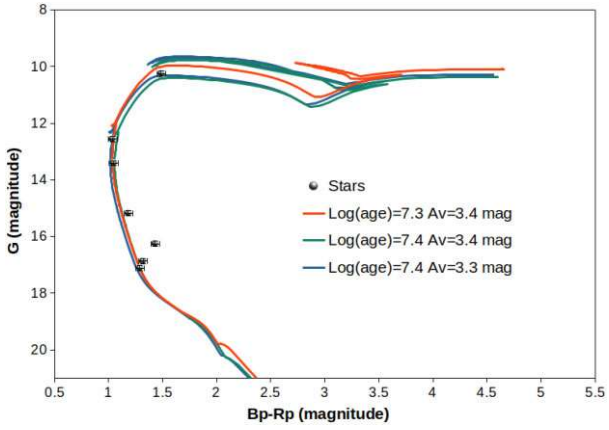

Figure 8. Isochrone fitting for the stars in the central region of SNR G126.2 + 1.6. The 20 Myr isochrone fits the massive stars well.

524 811 060 453 759 744 (B2) at 4160^{+199}_{-207} pc. The progenitor might be a member of a cluster together with these stars at an average distance of 4388^{+264}_{-253} pc. By an isochrone fitting for all the stars within 5 arcmin (6 pc) from the centre, with an average distance of 4396 ± 234 pc, we found a possible open cluster at an age of 20–25 Myr (Fig. 8). Assuming solar metallicity, the progenitor of the SNR has a mass of 12 $M_\odot$. The extinction towards the cluster is $A_V = 3.4$ mag. For SNR G126.2 + 1.6, we suggest a distance of 4.4 ± 0.3 kpc.

Like in the case of previous SNRs, the extinction has a steep rise to 3.0 mag, until 1.0 kpc. The trend line is rather flat until 5.0 kpc. The extinction at 4.3 kpc is 3.35 mag (Fig. 7).

The SNR has a physical radius of 44 pc. Assuming that it is in the radiative phase, from McKee & Ostriker (1977), we found an age of $\tau = 41000$ yr, for $E_0 = 10^{51}$ erg and $n_0 = 1$ cm^{-3}.

No OB-runaway star was found.

4.6 G127.1 + 0.5 (R 5)

R 5 is a shell type SNR with a diameter of about 45 arcmin (Kothes et al. 2006; Green 2009; Fig. 9). The shell is bright and complete in radio bands, while it is not recognized in optical bands. The H α emission is diffuse (Xilouris et al. 1993) and hardly related to the SNR. The central compact radio sources are confirmed to be extragalactic objects (Kirshner & Chevalier 1978).

The kinematic distance derived from −12 to −16 km s^{-1} velocities (Leahy & Tian 2006) is 1.15 kpc. The distance was also confirmed by the open cluster NGC 559 (Blair et al. 1980). However, more recent age and distance measurements for this cluster is 224 ± 24 Myr and 2.43 ± 0.23 kpc (Joshi et al. 2014). Due to the low surface brightness of the SNR, the Σ–D diagram gives a distance of 2.5 kpc (Guseinov et al. 2003). At the distance of 1.15 kpc, assuming that the initial explosion energy is $E_0 = 0.5 \times 10^{51}$ erg, the age was found as 20−30 kyr (Leahy & Tian 2006).

Although it is neither a candidate nor a runaway star, the O9.5IV type (Morgan et al. 1955) bright star, HD 8768, which is slightly out of the search region, was observed by FLECHAS. In the FLECHAS spectrum, blue-shifted component for the Na I–D1 and D2 lines is detected (Fig. B1). This indicates the star is either inside or behind the SNR, so it is a good distance indicator for R 5. The parallax measurement towards the star is not accurate. However, the star has a visual companion, HD 8768B (Maíz Apellániz 2010), which has a precise parallax measurement. Also there are other stars within only 2 arc min, which have a similar parallax. The progenitor star may be related to this group. Additionally, circularly distributed warm clouds, which are bright in MIR surround the SNR's north-northeastern part. The clouds host YSOs (Fig. 9). The star formation might have been triggered by the winds of the progenitor. The average distance of the YSOs and HD 8768 binary is 2591^{+271}_{-206} pc (Table C2). The open cluster NGC 559 is also at a similar distance. Yet, this cluster is far too old to host an SNR progenitor (τ >100 Myr). Shortly, the system at 2.6 kpc hosts massive stars and star formation, which is an expected environment for an SNR. Also, 2.6 kpc is favoured by the Σ−D diagram (Guseinov et al. 2003).

However, the SNR is faint in the south and the circular shape has been distorted severely in the south-west. The similar distortion is observed in SNR CTB 109 and is explained by the interaction with a GMC (Sasaki et al. 2006). Based on CGPS CO images, a GMC in the south-west is present at a systematic velocity of −13 km s^{-1} (Fig. 9). This is consistent with the found by Kothes et al. (2006) based on H I velocity corresponding to a distance of 1.15 kpc. The star-forming region Sh 2-187, 20 pc south of the SNR. A member star Sh 2-187 1 lies at a geometric distance of 917^{+7}_{-8} pc.

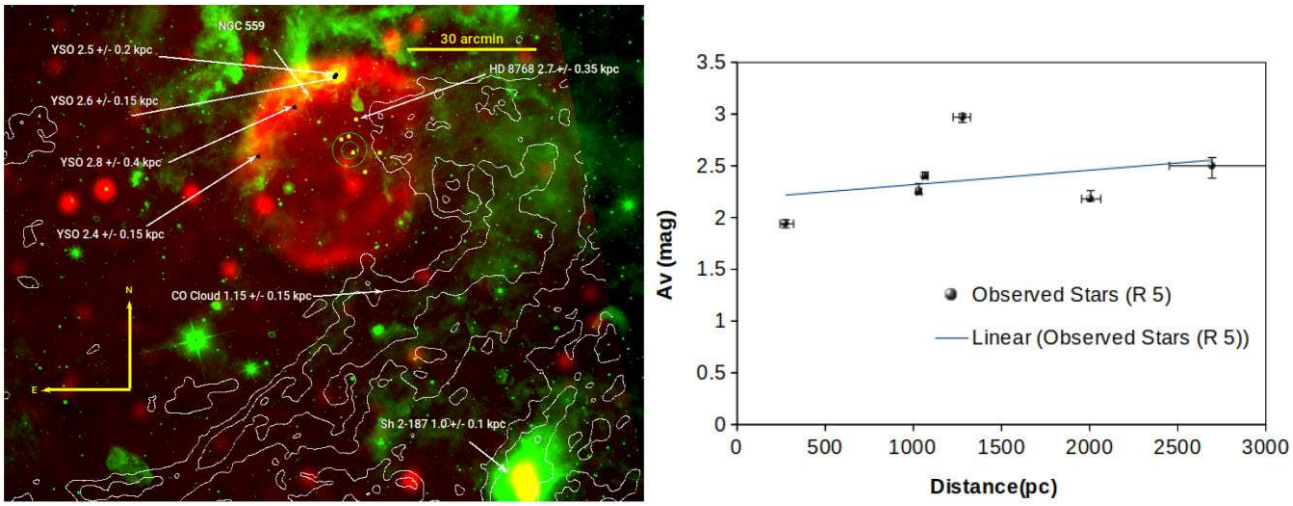

Figure 9. *Left*: Colour composite image of SNR R 5 and its surrounding. Red represents the 1420 MHz image from CGPS, while green is the *W*3-band image of *WISE* Survey, retrieved from *Skyview*. White contours overlaid is the CO map at -13km s^{-1}, taken from CGPS. Black dots shown are the massive YSOs, mostly transition disc objects that belong to the star formation regions inside the GMC. The rough geometric distances are given. The two green circles (big and small), in the middle of the SNRs, are the OB-runaway search region and the geometrical centre region. The yellow dots are the stars of which we have taken spectra and which were used for the determination of the A_V values. *Right*: Radial distribution of the extinction towards the central region of SNR R 5.

There is a striking difference between two distance estimates. The morphological disturbance can be explained by the molecular cloud interaction at 1.15 kpc. On the other hand, the SNR is very faint in X-rays, which implies a larger evolved SNR like S 147, suggesting a larger diameter. Interaction with the molecular cloud would generate a reverse shock, which heats and compresses the ejecta to give rise in the X-ray flux. Furthermore, the distortion might be due to the break-out like in the case of CTB 1. Therefore, we suggest a distance of 2.6 ± 0.3 kpc for SNR G127.1 + 0.5.

The shock radius at 2.6 kpc is 17 pc. The SNR must be expanding in a low density medium and has recently reached the denser region in the north, hence the northern part of the radio shell is significantly brighter than the southern filaments where there is no star-forming regions or molecular clouds, thus a less dense region. Assuming that the SNR is in its Sedov phase, we calculate an age of $\tau = 5100$ yr for $E_0 = 10^{51}$ erg and a low number density of $n_0 = 0.1$ cm^{-3}.

The extinction increases steeply due to the fore-ground and/or possibly interacting clouds (Fig. 9) even before 500 pc. At the suggested distance, 2.6 kpc, the extinction is, $A_V = 2.5$ mag.

The OB-runaway search was performed for parallaxes from 0.25 to 2.0 mas up to an extinction of $A_V = 4.0$ mag. No OB-runaway candidate was found.

4.7 G130.7 + 3.1 (SN 1181?)

G130.7 + 3.1 is a plerion type SNR with angular dimensions of about $9' \times 5'$ (Green 2009). The SNR is very faint, the emission is dominated by the energetic PWN. It was suggested to be the remnant of the new star recorded in AD 1181 (Stephenson & Green 2002). However, a discrepant age of 3000 − 5000 yr was determined for the nebula (Fesen et al. 2008). The neutral hydrogen column density of $N_H = (3.75 \pm 0.11) \times 10^{21}$ cm^{-2} (Slane, Helfand & Murray 2002) was derived from CHANDRA observations of the pulsar; a distance of 3.2 kpc was suggested from the H I velocity of -35 km s^{-1} (Roberts et al. 1993). Considering the density wave pressure in this direction, similar to HB 3, the distance was estimated as 2.0 kpc (Kothes 2013). A DM of 140.7 ± 0.3 pc cm^{-3} (Camilo et al. 2002) suggests a distance of 2.8 kpc (Yao, Manchester & Wang 2016). The total visual absorption is $A_V = 1.6$–2.3 mag, consistent with the N_H (Fesen et al. 2008).

The spin period and period derivative of the pulsar is $P = 65.68$ ms (Bietenholz et al. 2013) and $\dot{P} = 1.93 \times 10^{-13}$ s s^{-1} (Livingstone et al. 2009). This corresponds to a characteristic age of $\tau = 5380$ yr and $B_{dip} = 3.6 \times 10^{12}$ G. Yet the SNR age is $\tau \sim 840$ yr, assuming the historical record. The age discrepancy can be explained by high initial spin period (Murray et al. 2002). However, as mentioned above, the SNR can also be at a comparable age with ∼5000 yr. This SNR is also far away from known OB associations and star formation regions. Recently, Ritter et al. (2021) suggested a different remnant for SN 1181, namely IRAS 00500 + 6713. However, to confirm the SNR nature of a nebula, a high percentage of radio polarization, a radio spectral index of 0.3–0.8, and a ratio of S II (λ6717 + λ6731) to H α (λ6562), higher than 0.5 are needed, and a radio counterpart of a possible shock wave of IRAS 00500 + 6713 is missing and the [S II/H] ratio is not mentioned. The nebula was suggested to be an SNR originated from a Type Iax SN, based on the possible super-Chandrasekhar point source in the centre (Oskinova et al. 2020).

No OB-runaway candidate was found inside the SNR up to an extinction of $A_V = 3$ mag and a distance of 5 kpc.

4.8 G132.7 + 1.3 (HB 3)

HB 3 is a MMSNR with an angular diameter of about 80 arcmin (Green 2009). It resides in a complex region with an asymmetric shape in radio bands (Fig. 10). It is possibly interacting with the molecular clouds of *W*3 in the south-east (Routledge et al. 1991). The shell is faint in optical bands and not observable in X-rays. The expansion velocity derived from diffuse H α emission is 150−180 km s^{-1} (Lozinskaia 1980). The dense filaments have velocities lower than 100 km s^{-1} indicating that HB 3 is an evolved SNR. The A_V, measured from optical filaments, is 2.2 ± 0.1 mag (Fesen et al. 1995), while the N_H towards the central region derived from the X-ray spectrum is $(9.2 \pm 0.6) \times 10^{21}$ cm^{-2}, which corresponds to ∼4.5 mag A_V (Lazendic & Slane 2006). The X-ray radiating plasma is at relatively low temperature, 0.14 ± 0.04 keV, which translates to $v_{bw} = 340$−400 km s^{-1}. Based on Sedov or

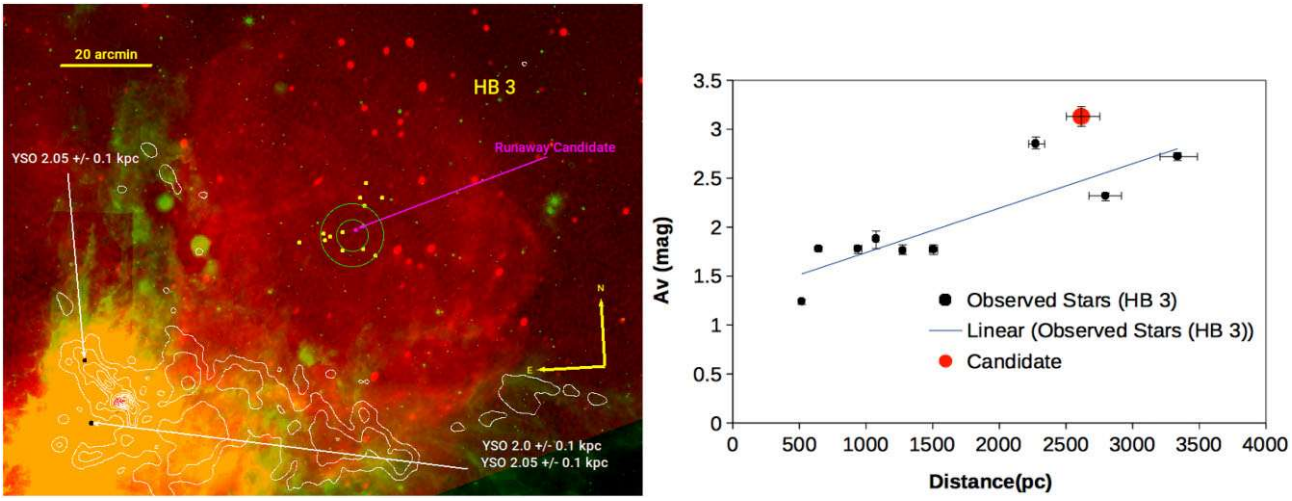

Figure 10. *Left*: Colour composite image of SNR HB 3 and the surroundings. Red represents the 1420 MHz image from CGPS, while green is the *W*3 band image of *WISE* Survey, retrieved from *Skyview*. White contours overlaid is the CO map at -42 km s^{-1}, taken from CGPS. Black dots show are the massive YSOs, mostly transition disc objects which belong to the star formation regions inside the GMC. The rough geometric distances are given. The two green circles (big and small), in the middle of the SNR are the OB-runaway search region and the geometrical centre region. The yellow dots are the stars of which we have taken spectra and which were used for the determination of the A_V values. *Right*: Radial distribution of extinction towards the central region of SNR HB 3. The star *Gaia* DR3 513 927 750 767 375 872 shows a compatible A_V value for an OB-type star.

evaporating cloud models, $E_0 = (0.3{-}2.0) \times 10^{51}$ erg and $\tau = 30000 \pm 5000$ yr at 2.2 kpc. The diameter of HB 3 at this distance is 51 pc. Enhanced abundances in Mg is possible. Hence, HB 3 is an old SNR which is most likely to have a core-collapse origin (Lazendic & Slane 2006).

The systematic velocity of H I related to the SNR was found as -30 km s^{-1} (Read 1981; Routledge et al. 1991). The CO clouds detected by 408 MHz observations, which might be shocked by the SNR has -43 km s^{-1} velocity, while the systematic velocity of *W*3 from 1720 MHz OH Maser observations is -40 ± 5 km s^{-1} (Koralesky et al. 1998). The average velocity of H α filaments is -45 ± 3 km s^{-1} (Lozinskaya 1981). The corresponding distances are 2.3 (from H I), 3.4 (from *W*3) and 4.0 (from H α) kpc. The distance of the full extent of the complex, $l = 132^\circ{-}138^\circ$ considering the OB stars and H II regions, is 2.0 ± 0.05 kpc (Xu et al. 2006; Kiminki et al. 2015). The distance derived from the Σ–D diagram is 1.93 kpc (Guseinov et al. 2003).

From three massive YSOs, we derived a distance of 2027^{+78}_{-81} pc for *W*3 region (Table C2; Fig. 10). We also found a massive star close to the central region. The star *Gaia* DR3 513 935 236 883 563 392 (B3) is at a geometric distance of 2274^{+65}_{-54} pc (Table C1). Therefore, a distance of $d = 2.1 \pm 0.2$ kpc would be plausible for HB 3 (Fig. 10).

We searched for an OB-runaway star inside HB 3 up to an extinction of $A_V = 4$ mag and a distance of 4 kpc and found a candidate. The star *Gaia* DR3 513 927 750 767 375 872 lies in the inner search region (Fig. 11), at a geometric distance of 2615^{+138}_{-113} pc. At this geometric distance, the star can have an effective temperature of $16000 \leq T \leq 21000$ K, a surface gravity of $4.25 \leq \log(g) \leq 4.31$ with an extinction of $3.0 \leq A_V \leq 3.2$. Although the extinction is higher than the mean average from the linear fit, the high extinction of one of the reference stars, *Gaia* DR3 513 935 236 883 563 392 implies the target star can be a good candidate.

The *Gaia* DR3 proper motion of the star is $\mu^*_\alpha = -3.3 \pm 0.1$ and $\mu_\delta = 1.1 \pm 0.2$ mas yr^{-1}, which is obviously different from those of the young stars of the region, i.e. the B3-type star we found shows a typical proper motion of $\mu^*_\alpha = -1.0 \pm 0.1$ and $\mu_\delta = -0.19 \pm 0.1$ mas yr^{-1}. Correcting for Galactic rotation and solar peculiar motion, the proper motion becomes $\mu^*_\alpha = -2.3 \pm 0.1$ and $\mu_\delta = 1.2 \pm 0.2$ mas yr^{-1} which translates to a 2D space velocity of 33 ± 3 km s^{-1}. The star is located in the geometrical centre region. Tracing back the corrected proper motion for 30 kyr, a conservative estimate for the age, we find that the star is still within the geometrical centre region – and it approaches to the centre. Despite the small discrepancy between the distances of the SNR and our *Gaia* runaway candidate, the star is an OB-runaway candidate, the pre-SN companion candidate to the progenitor of HB 3. Unfortunately, the spectral type could not be determined by Subaru FOCAS observations because of the low signal-to-noise ratio due to weather conditions.

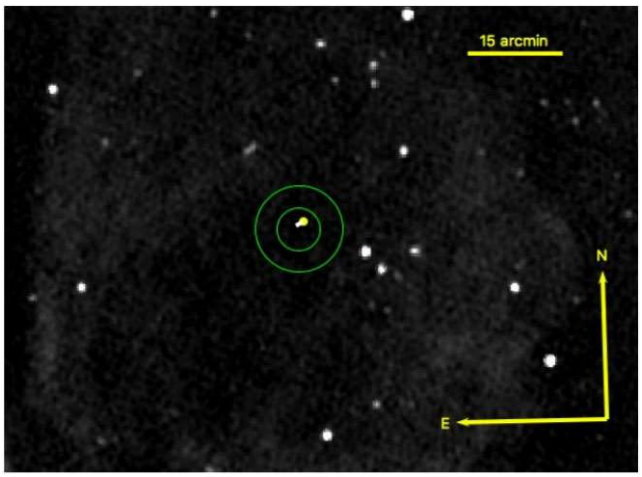

Figure 11. The vector of proper motion of the OB-runaway candidate (yellow spot) inside HB 3 is traced back for 30 kyr (white lines), and the star still lies in the central region.

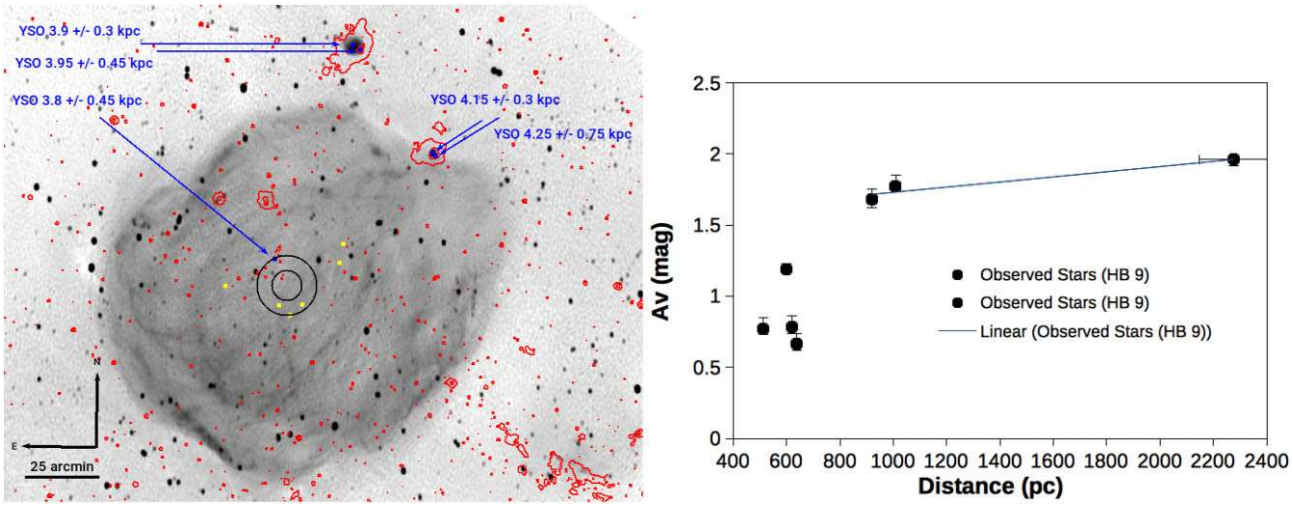

Figure 12. *Left*: 1420 MHz image of SNR HB 9 from CGPS. The two black circles (big and small), in the middle of the SNR are the OB-runaway search region and the geometrical centre region. The yellow dots are the stars of which we have taken spectra and which were used for the determination of the A_V values. The blue dots are the YSOs and massive stars in the direction of the SNR. The red countours represent the *W*3-band image of *WISE* survey. *Right*: Radial distribution of the extinction towards the central region of HB 9.

The extinction towards the central region of the SNR varies between 1.5 and 3.0 mag, from 0.5 to 3.5 kpc.

We suggest two possible distance to the SNR. From W3 region and the massive star, we found close to the centre, the distance is 2.1 ± 0.2 kpc and if the OB-runaway candidate is confirmed to be an OB-type star, then it will be revealed that the progenitor of the SNR was behind the system at 2.6 ± 0.15 kpc.

4.9 G160.9 + 2.6 (HB 9)

HB 9 is a MMSNR with an angular size of about 140 arcmin × 120 arcmin (Green 2009). It is centrally filled in X-rays, while the shell is bright in radio and partially bright in optical bands. The systematic velocities found for the H I clouds are −3 to −9 km s^{-1}, which corresponds to a distance of 0.8 ± 0.4 kpc (Leahy & Tian 2007), and -18 ± 10 km s^{-1}, which is at 2.8 ± 0.8 kpc based on H α observations (Lozinskaya 1981). The N_H determined from ROSAT X-ray observations is very low, 2.7×10^{20} cm^{-2}. This is even lower than the A_V derived from the optical filaments, which is 0.6 ± 0.25 mag (Fesen et al. 1985). The temperature derived is $T \sim 0.8$ keV, meaning a shock velocity of ∼900 km s^{-1} (Leahy & Aschenbach 1995). The age is suggested to be 4000–7000 yr (Leahy & Tian 2007).

The star-forming regions in this direction are far from the suggested distances. The young H II regions Sh2 − 219 and Sh2 − 217 and another YSO (Fig. 12) in the central region lie at an average distance of d= 4008^{+462}_{-367} pc (Table C2). The radius of the SNR is 70 pc at 4.0 kpc, which is much larger than the any SNR in our sample. Also, the surface brightness is much larger than a possible SNR with that radius. Therefore, this value of distance does not seem plausible. We cannot connect the SNR any structure, so we do not mention any estmation.

We measured the extinction up to 2.5 kpc. The extinction at 0.8 kpc we found is ∼1.4 mag (Table C1), which is larger than proposed values so far. For the future X-ray observations, this value should be taken into account.

We searched OB-runaway stars as a potential pre-SN binary companion to the SNR for a maximum extinction of $A_V = 3$ mag and a distance of d=2.0 kpc. There is no OB-runaway star for HB 9.

4.10 G166.0 + 4.3 (VRO 65.05.01)

VRO 42.05.01 is a MMSNR composed of two hemispheres with great differences in diameter, 55 arcmin × 35 arcmin (Green 2009), see Fig. 13. The shell is bright in radio and optical bands, while centrally filled in X-rays. This peculiar morphology is explained by breakout to the low density medium in the west (Pineault, Landecker & Routledge 1987). In the X-ray spectrum from *XMM–Newton* observations, no enhanced chemical abundance was found. The blast wave velocity inferred from the plasma temperature of $T = 8.5 \times 10^6$ K is $v_{bw} = 680$ km s^{-1} (Bocchino, Miceli & Troja 2009). Based on H α radial velocities, the expansion velocity was measured as 200 km s^{-1} (Lozinskaia 1979a).

The velocity V_{LSR} of the H I clouds was measured as -31 ± 5 km s^{-1} (Landecker et al. 1989). But, due to the Perseus arm velocity anomaly (see Section 4.8), the systematic velocity is not a good indicator in this direction, it only shows that the distance is above 1.8 kpc. For a flat rotation curve, such a high negative velocity does not exist. The SNR was thought to be an outer-arm object with a distance of 4.5 ± 1.5 kpc (Landecker et al. 1989). The Σ–D diagram suggests a distance of 3.9 kpc (Guseinov et al. 2003).

The A_V is 1.68 mag (Fesen et al. 1985). The N_H derived from the X-ray spectrum are also low, 2.9×10^{21} cm^{-2} (Guo & Burrows 1997) or $(1.3–2.6) \times 10^{21}$ cm^{-2} (Burrows & Guo 1994).

HD 278115 is a massive star (B1V) outside of our search region (Fig. 13). The TRES spectrum shows highly red-shifted and blue-shifted components for Ca II-K and H lines (Figs. B2 and B3). We measured the ISM line velocities by fitting multicomponent Gaussian using IRAF's *deblending* task. The velocities measured for Na I-D1 and D2 lines are between −22 to +14 km s^{-1}, while Ca II-K and H show high velocities, between −101 and +140 km s^{-1} (Table 5).

The absence of very high-velocity components of Na I-D1 and D2 lines show a higher temperature, hence the lines are due to the SNR expansion. So, the star is definitely a background object to

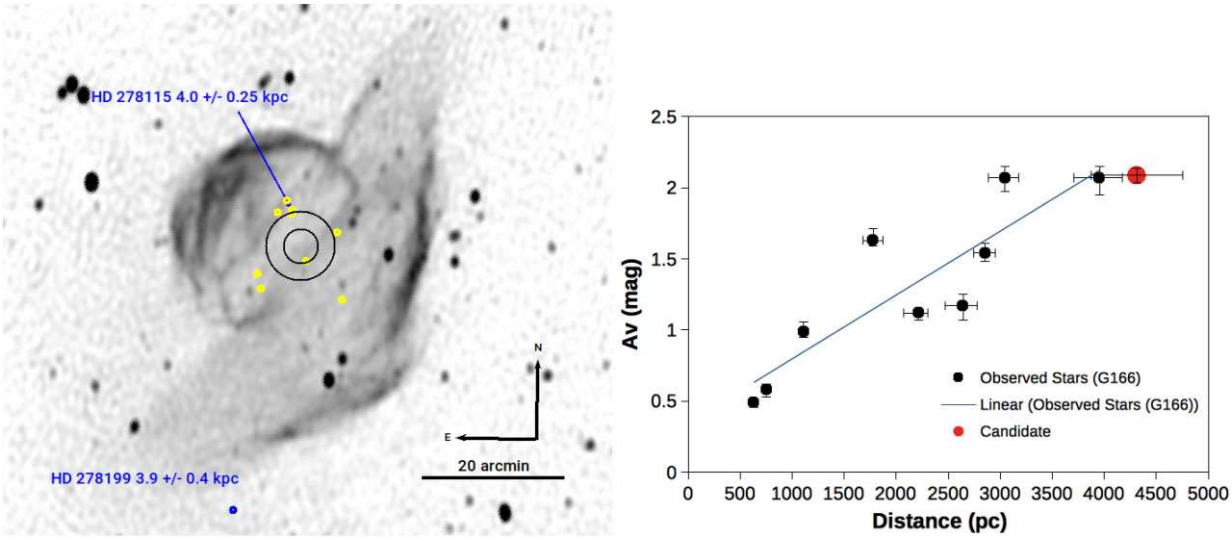

Figure 13. *Left*: 1420 MHz image of SNR G166.0 + 4.3 from CGPS. The two white circles (big and small), in the middle of the SNRs, are the OB-runaway search region and the geometrical centre region. The yellow dots are the stars of which we have taken spectra and which were used for the determination of the A_V values. The blue dots are the massive stars that we searched for high-velocity ISM component in their spectra. *Right*: Radial distribution of the extinction towards the central region of SNR G166.0 + 4.3. The candidate star (red) *Gaia* DR3 195 632 152 560 621 440 has a minimum compatible minimum A_V value with the extinction determined by the observed stars.

Table 5. Velocities measured for Na I–D1 and D2 and Ca II–K and H ISM lines towards HD 278115. Values are in km s^{-1}.

Na I–D1	Na I–D2	Ca II–K	Ca II–H
−21, +14	−22, +13	−98, −78, +22, +125, +140	−101, −79, +20, +123, +140

VRO 42.05.01. This is surely a good tool to set an upper limit to the SNR distance.

The geometric distance to the star is 3955^{+258}_{-220} pc. Another possible SN progenitor within 1° is HD 278199 (B3V) (Cannon & Mayall 1949) at a geometric distance of 3889^{+438}_{-308} pc. This strengthens the idea that the SNR is also at ∼3.9 kpc. As HD 278115 is a background star, the upper limit of the SNR distance is 4.2 kpc. Therefore, a distance of 3.9 ± 0.3 kpc could be a conservative approach.

At 3.9 kpc, the larger radius of the SNR is 31 pc, while the smaller is 20 pc. Using $R = 31$ pc and $v_{bw} = 680$ km s^{-1}, the age of the SNR from Sedov solution is 18 000 yr. This corresponds to a high E_0/n_0 ratio, which is 18. For a canonical explosion energy of $E_0 = 10^{51}$ erg, the ambient medium density is $n_0 = 0.055$ cm^{-3}. The medium in which the northeastern part of the SNR is expanding has a ten times larger ($n_0 = 0.55$ cm^{-3}) density, assuming the same age but a smaller radius of the SNR.

The extinction we found is A_V ∼2.1 mag at 3.9 kpc, slightly larger than the literature values.

We searched for OB-runaway stars between parallaxes of 0.2–0.6 mas for a maximum extinction of 3.0 mag (Fig. 14). *Gaia* DR3 195 632 152 560 621 440 satisfied both the kinematical and temperature criteria. However, the Subaru FOCAS spectrum reveals that the target is an evolved A3 type star. The star can be much older than a progenitor star, thus it cannot be the pre-SN binary companion. Spectral type estimation from photometry has large uncertainties. Early A type stars cannot be excluded easily. On the other hand, if a star is truly an OB-type star, then it would not be excluded.

4.11 G184.6−5.8 (Crab Nebula)

Crab Nebula is another plerion type SNR in the sample with a small angular diameter of about 9 arcsec (Green 2009). It is the only candidate for the historical SN in 1054 A.D. (Stephenson & Green 2002). The ejected mass is 1−2 $M_\odot$, and the swept up mass (2−3 $M_\odot$) is still comparable with the mass of the ejecta (MacAlpine & Uomoto 1991). The measured velocities from bright filaments, <2000 km s^{-1} (Clark et al. 1983), implying a low explosion energy of $E_0 = 3.2 \times 10^{49}$ erg (Fesen, Shull & Hurford 1997a). The extinction measured from the optical nebula is $A_V = 1.6 \pm 0.2$ mag (Miller 1973). Based on the abundances derived from the optical spectra, the progenitor zero-age main sequence mass is proposed to be >9.5 $M_\odot$ (MacAlpine & Satterfield 2008), or 8−10 $M_\odot$ (Davidson & Fesen 1985).

The period and period derivative of the Crab pulsar are $P = 33$ ms and $\dot{P} = 4.21 \times 10^{-13}$ s s^{-1} (Lyne et al. 2015). The corresponding magnetic field and characteristic age are $B_{dip} = 3.79 \times 10^{12}$ G and $\tau = 1260$ yr. It does not show a large characteristic age anomaly. Various indicators suggest a distance of 2.0 ± 0.5 kpc (Trimble 1973; Kaplan et al. 2008).

The Crab Nebula has a large separation from the known OB associations and star formation regions. There is no OB association within 300 pc from the remnant. There is also no OB stars inside or in the close vicinity of the SNR. There are a number of late-type stars close to the geometrical centre of the SNR, but none of them is the pre-SN binary companion to the progenitor (Fraser & Boubert 2019). It is clear that the progenitor of Crab was formed in isolation or migrated to the current position, and gave birth to an energetic pulsar by a weak SN. In this regard, it may be similar to G130.7 + 3.1.

The geometric distance to the pulsar is 1961^{+389}_{-253} pc. The proper motion values are, $\mu^*_\alpha = -11.51 \pm 0.10$ and $\mu_\delta = +2.30 \pm 0.06$ mas yr^{-1}. The space velocity of the pulsar is 94.1−132.0 km s^{-1}.

No runaway candidate is found and no spectroscopic observation was performed towards this SNR.

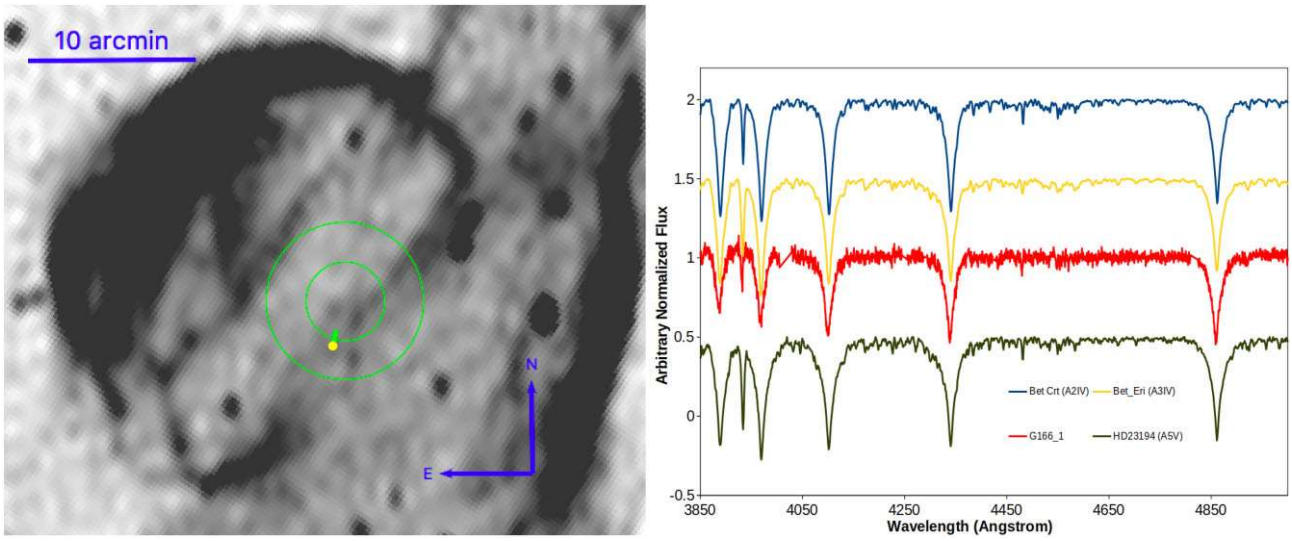

Figure 14. *Left*: The vector of proper motion of the OB-runaway candidate (yellow spot) inside G166.0 + 4.3 is traced back for 60 kyr (white lines). The star lies in the central region. *Right*: Subaru/FOCAS spectrum of the OB-runaway candidate *Gaia* DR3 195 632 152 560 621 440 (G166_1 in the figure). A deep Ca II−K line and the lack of any He lines shows that the star is definitely not an OB-type star. The spectrum is compatible with an A3IV type.

4.12 G189.1 + 3.0 (IC 443)

IC 443 is an MMSNR (Rho & Petre 1998) with an angular diameter of about 45 arcmin, located at the Galactic anticentre direction (Green 2009). The SNR shell is bright and shows the same morphology in radio, X-ray, and optical wavebands (Fesen 1984; Asaoka & Aschenbach 1994; Leahy 2004). It also shows a centrally peaked morphology in X-rays (Petre et al. 1988). Unlike other MMSNRs, the central X-ray emission originates from two different positions, in the north and in the centre (Troja et al. 2008), suggesting a cloud evaporation origin. The shock wave is interacting with the surrounding dense atomic and molecular clouds (Claussen et al. 1997; Snell et al. 2005) and expanding in a highly inhomogeneous environment. Hence, it is comprised of two semi-spherical shells sharing the same horizontal plane but having different radii and centroids (Fig. 15).

Based on the genetic connection with the Gem OB1 association (Humphreys 1978) and Sh 2-249 H II region (Galt & Kennedy 1968), the distance estimation to the SNR is ∼1.5 kpc. Due to the high temperature (10^7 K) of the plasma in the north eastern rim, the suggested age is 3 kyr (Petre et al. 1988). Another young age, 4−10 kyr, was derived based on the radius comparison of the southern shell and the possible ejecta ring (Troja et al. 2008). It is suggested as 10−20 kyr, considering its mixed morphology nature (Kawasaki et al. 2005).

The shock velocities measured from the filaments in the optical bands are in the range of 60−100 km s^{-1} (Lozinskaya 1969; Fesen & Kirshner 1980). Also velocities up to 350 km s^{-1} from diffuse H α emission was detected by long-slit spectroscopy. Taking the projection effects into account, a shock velocity of 400 km s^{-1} was suggested (Lozinskaia 1979b). The Sedov solution gives an age of 60 and 10 kyr for the low and high velocities measured. Considering an SNR evolution within the low density bubble owing to the fast winds of the progenitor and the neighbouring stars, the age was estimated as 30 kyr (Chevalier 1999).

The A_V value measured from H β/H α strength ratios is 2.5−3.4 mag (Fesen 1984), which is consistent with the $N_H \sim 6.2 \times 10^{21}$ cm^{-2}, measured in X-ray spectra (Troja et al. 2008). Furthermore, from NIR Fe II line intensities, it is found that A_V varies from 2 to 6 mag within the northeastern shell (Kokusho et al. 2013).

The compact object of the SNR is the NS CXOU J61705.3 + 222127. Although it shows no radio emission, its PWN and blackbody radiation are observable in X-rays (Bocchino & Bykov 2001; Olbert et al. 2001). No pulse has been detected so far. From the hydrogen atmosphere model, the effective temperature was found as $T_{\rm eff} \approx 6.8 \times 10^5$ K. The blackbody model yields a higher temperature, $T_{\rm eff} \approx 1.6 \times 10^6$ K, close to that of the Vela pulsar (Swartz et al. 2015), a 10−30 kyr old NS. The cooling age is consistent with the SNR age of 30 kyr (Gaensler & Slane 2006). The X-ray bolometric luminosity of the PWN is $L_{\rm PWN} \approx 1.4 \times 10^{33}$ erg s^{-1}. Based on this value, the predicted period of the pulsar is $P = 250$ ms with a relatively high magnetic field strength, $B_{\rm dip} = 2.0 \times 10^{13}$ G. Overall, it is an energetic pulsar with a possible spin-down luminosity of $\dot{E} = (1 - 30) \times 10^{36}$ erg s^{-1}. The position of the NS is ∼12 arcmin separated from the geometrical centre of IC 443 to the south. The proper motion in RA and Dec. was measured as $\mu_\alpha^* = -18.1 \pm 33.4$, $\mu_\delta = -1.2 \pm 33.4$ mas yr^{-1} (Swartz et al. 2015). Seven other members (Mel'Nik & Efremov 1995) of Gem OB1 were observed by us with FLECHAS. FLECHAS observations showed that three stars behind the SNR, HD 43582 HD 254477, and HD 254577, display high-velocity components for the interstellar Na I–D1 and D2. All these components are blueshifted and very strong. Especially in the spectrum of HD 254477, the high-velocity component is nearly at the same strength of the component at $V_{\rm LSR} \approx 0$ km s^{-1} (Fig. 16). Other investigations in the literature have reported that the components at negative velocities are much more intense than those at positive velocities (Welsh & Sallmen 2003; Hirschauer et al. 2009). Therefore, the dense medium is one-sided, between the explosion centre and the observer.

The extinction rises steeply at around 1.7 kpc, where the massive stars are located. The SNR is clearly interacting with the molecular cloud and is behind it. Therefore, the significant difference in the extinction between the stars marks the location of the SNR, which is 1500–1750 pc. We suggest a conservative distance of 1.6 ± 0.15 kpc for IC 443, not much different from the previous estimate, but more precise.

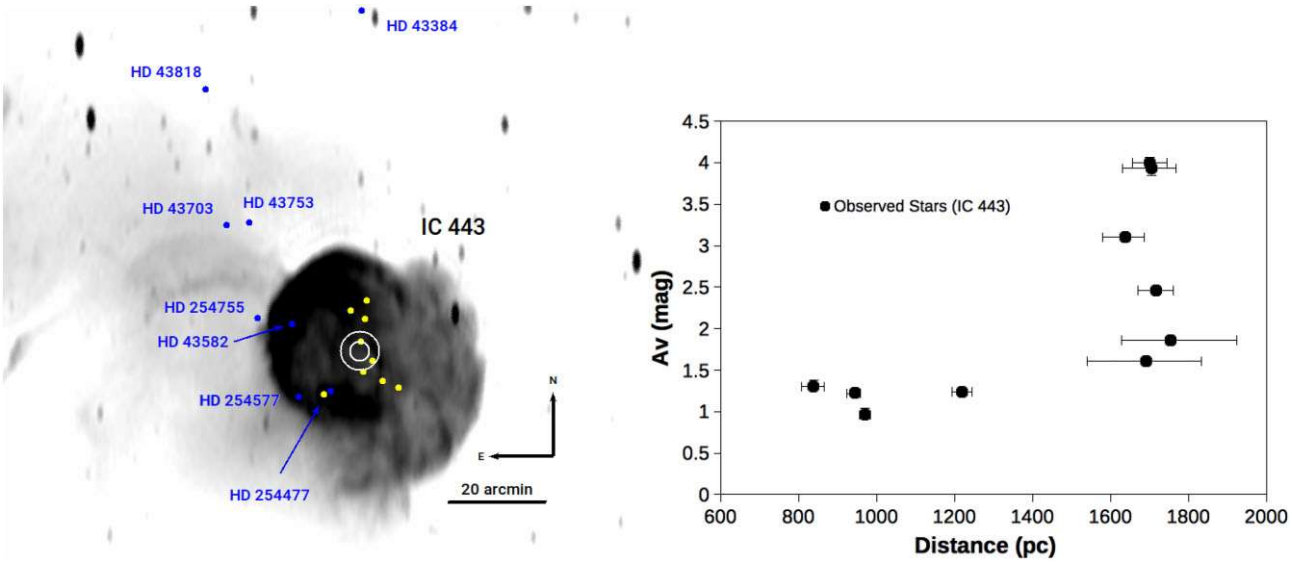

Figure 15. *Left*: 1420 MHz image of SNR IC 443 from CGPS. The two white circles (big and small), in the middle of the SNR are the OB-runaway search region and the geometrical centre region. The yellow dots are the stars of which we have taken spectra and which were used for the determination of A_V values. The blue dots are the massive stars that we searched for high-velocity ISM component in their spectra. *Right*: Radial distribution of extinction towards the central region of IC 443.

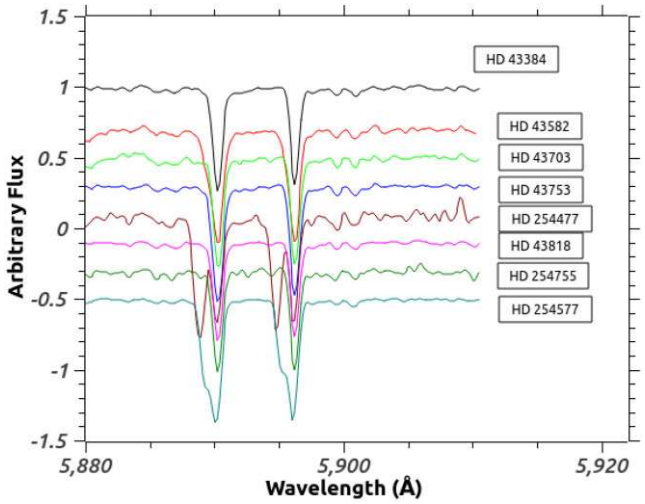

Figure 16. FLECHAS spectra of eight massive stars. Three stars, HD 43582 HD 254477 and HD 254577, display high-velocity component for the ISM Na I–D1 and D2.

Although the massive progenitor is quite clear, there is no OB-runaway star inside IC 443 up to an extinction of $A_V = 4.0$ mag and a distance of $d = 3$ kpc.

5 SUMMARY AND DISCUSSION

Twelve well-studied SNRs are searched for an OB-runaway star as a pre-SN companion to the progenitor. The SNR distances are widely discussed to check the distance consistency between the target stars and the SNRs. Also the extinctions towards the central regions of the SNRs are set through a large distance interval. Stars are selected by positional, kinematic, and temperature criteria. The search was performed within the central sixth of the SNR radius, among the stars whose distances are within the distance interval of the SNRs. The transverse velocity, derived from the *Gaia* DR3 proper motion and parallax values of the stars, is expected to be higher than 17.6 km s^{-1}, and the corrected proper motion vector must be pointing away from the geometrical centre of the SNR. The temperatures of the stars satisfying these conditions were estimated by *Gaia* G_{BP} G G_{RP} and 2MASS JHK$_s$ photometry. Those having a maximum temperature estimate higher than 10 000 K are selected and exposed to an extinction comparison with the SNRs. Those showing extinction values higher than the spectroscopically confirmed stars are most probably cooler stars and are eliminated. Out of 12 SNRs, two stars in total, inside the SNRs HB 3 and G166.0+4.3 are identified as OB-runaway star candidates. The star inside SNR G166.0 + 4.3 was found to be an A3-type sub-giant star (not an OB-runaway star) by Subaru FOCAS.

Gaia DR3 513 927 750 767 375 872 is the only OB-runaway candidate, which needs to be confirmed by spectroscopic observations. However, from the interaction with the molecular cloud, the distance to the SNR HB 3 seems to be 2.1 ± 0.2 kpc, while the candidate is at ∼2.6 kpc. In addition, the extinction estimated to the star is well above the average. Hence, the star is not a very strong candidate. It is possible that the star is instead an evolved A type star at the same distance. Also, in the *Starhorse 2* catalogue (Anders et al. 2021), the effective temperature is estimated as $T_{eff} = 9966^{+1039}_{-2132}$ K, with a surface gravity of $log(g) = 3.87^{+0.13}_{-0.17}$ in cgs, supporting this possibility. Therefore, the age of the star is well above the limits to be a pre-SN companion to a young progenitor.

As a result of our study, we did not find a massive OB-runaway star as pre-SN companion to the progenitor in a sample of 12 well-studied SNRs. A number of reasons might be proposed, we divided them into two parts; the selection effects due to our method and observational aspects, and physical reasons.

In our method, we cannot detect the OB-runaway stars ejected only in the radial direction as we expect a 2D space velocity of $v \geq 17.6$ km s^{-1} to clarify a star as candidate. Also, for certain reasons, the photometric and astrometric values of a star can be inaccurate. One possible reason of poor astrometry is binarity. As OB-runaways are mostly single stars, this does not disturb our search.

Table 6. SNR distances estimated, extinctions measured, and progenitors estimated in this work.

Name	Dist (pc)	Dist origin	A_v at dist.	Progenitor
G109.1 − 1.0	3.1 ± 0.15	SFR, MC	1.6 ± 0.2	Merger?
G114.3 + 0.3	2.85 ± 0.35	SFR, PSR DM, Polar	2.8 ± 0.3	Lower mass
	or 1.65 ± 0.2	–	–	–
G116.9 + 0.2	3.1 − 4.5	Assoc./MS	1.7 ± 0.2	Lower mass
G127.1 + 0.5	2.6 ± 0.3	MS, SFR, Bkg. St.	2.5 ± 0.5	O-type
G126.2 + 1.6	4.3 ± 0.3	MS, OC	3.2 ± 0.1	12 $M_\odot$
G130.7 + 3.1	4.55 ± 0.45	MS		–
G132.7 + 1.3	2.1 ± 0.2	Assoc. or runaway	2.5 ± 0.5	–
	or 2.6 ± 0.15	–		–
G166.0 + 4.3	3.9 ± 0.15	MS	2.0 ± 0.2	Lower mass
G184.6 − 5.8	1.95 ± 0.35	PSR Plx		–
G189.1 + 3.0	1.6 ± 0.15	MC, MS, Bkg. St.	3.0 ± 1.0	O-type

Note. MC = molecular cloud, MS = massive star, OC = open cluster, SFR = star-forming region, Assoc. = OB association, Bkg St. = background star, DM = dispersion measure.

The first astrophysical reason might be that the geometrical centres of the SNRs are located far from the real explosion centre. The SNR shock wave expands spherically symmetric in a homogeneous medium, yet the ambient medium may have different densities in different directions. Therefore, the SNR shape can be highly distorted by the ISM. This shifts the geometrical centre from the true centre where the explosion had occurred. However, this is not the case for S 147 (Dinçel et al. 2015), where the explosion centre, found from tracing back both the pulsar and the OB-runaway star, is located well within the geometrical centre region. This may not hold for other SNRs.

Second reason is that a large portion of the pre-SN binary companions are ejected as slower, walk-away stars owing to the large binary separation. For example, among the main-sequence secondaries, the walk-away fraction is suggested to be as large as ∼95 per cent in Renzo et al. (2019). We note that they set the velocity lower limit for runaway stars as 30 km s^{-1}. We search for stars faster than 17.6 km s^{-1} in 2D. Search for OB-runaway stars also tests the statistical results. For example, the possibility of finding a binary SN OB-runaway star like HD 37 424 is very low as it is a highly massive 13−19 $M_\odot$ (Kochanek 2021), and fast moving $v_{pec} = 74 \pm 8$ km s^{-1} (Dinçel et al. 2015) star. However, it was discovered by applying the methods explained in this work.

A third point is that the mass fraction can be low, i.e. $q = 0.2$. Searching for OB-runaways include stars having an effective temperature of $T_{eff} > 10\,000$ K, considering solar metallicity, the mass of such stars is 2.5 $M_\odot$. For a low-mass progenitor (∼8 $M_\odot$), the companion has a mass of 1.6 $M_\odot$ for $q = 0.2$. Low-mass stars can also be searched inside the SNRs but to prove that they are pre-SN companions is difficult, as the chance projection possibility is much higher and the age determination of these stars is challenging. On the other hand, some (22^{+26}_{-8} per cent in Renzo et al. 2019) of the close binaries end as a merger, which does not yield a runaway star.

The last reason is an observational selection effect of the SNRs. The Galactic SN rate is $2.5^{+0.8}_{-0.5}$ SNe per century (Tammann, Loeffler & Schroeder 1994). Considering a 100 kyr lifetime for the SNRs, the number of observable SNRs today, would have been ∼2500, while it is only ∼300 (Green 2009), 10−15 per cent of the expected number. The rate of OB-runaway stars to all OB-type stars is somewhat larger than this ratio, 20 per cent. Hence, it is also possible that some of the progenitors can be OB-runaway stars, which in general do not have a companion. As they move out of the large bubbles of the OB associations, it is more likely to detect their SNRs as they can interact with a relatively homogenous and reasonably dense ($n \sim 1$ cm^{-3}) ambient medium. OB-runaways like HD 37 424 might have experienced a two-step ejection, where a massive binary is first dynamically ejected from a cluster, and then the secondary is ejected by a binary SN (Pflamm-Altenburg & Kroupa 2010). Betelgeuse is also suggested to have had such an origin (Neuhäuser et al. 2022). In our sample, only IC 443 can guarantee that its progenitor is not a runaway star, but a member of Gem OB1 association.

In this work, we also determined distances, ages, and extinctions for the studied SNRs, and they are given in Table 6.

To summarize, a combined effect of these factors may cause the low (observed) rate of OB-runaway stars inside SNRs.

ACKNOWLEDGEMENTS

This work was conceived by the late Oktay H. Guseinov (1938–2009). We acknowledge the leading role he had in all stages of this work and other related topics. His contribution to Galactic Astrophysics and his scholarship will be greatly missed. We thank Ed van den Heuvel and Ulrich Heber for their support and fruitful discussions. This work is based on observations obtained with telescopes of the University Observatory Jena, operated by the Astrophysical Institute of the Friedrich-Schiller-University Jena. We appreciate the observational support from Daniel Wagner, Martin Seeliger, and Kim Werner. This research has made use of ALADIN, Skyview, and CDS data base. We would like to thank the Calar Alto observatory staff for their help in our observations; and we would like to thank DFG in NE 515/53-1 for financial support for the Calar Alto observing run. This research is based on data collected at the Subaru Telescope, with run ID: S22A0154S, which is operated by the National Astronomical Observatory of Japan. We are honoured and grateful for the opportunity of observing the Universe from Mauna Kea, which has the cultural, historical, and natural significance in Hawaii. We also thank TÜBİTAK National Observatory for their supports in using RTT-150 with project number 12ARTT150-267.

DATA AVAILABILITY

The data underlying this article will be shared on reasonable request to the corresponding author.

REFERENCES

Allakhverdiev A. O., Guseinov O. H., Tagieva S. O., Yusifov I. M., 1997, Astronomy Reports, 41, 257
Anders F. et al., 2021, A&A, 658, A91
Anderson M., Rudnick L., Leppik P., Perley R., Braun R., 1991, ApJ, 373, 146
Ankay A., Kaper L., de Bruijne J. H. J., Dewi J., Hoogerwerf R., Savonije G. J., 2001, A&A, 370, 170
Arzoumanian Z., Chernoff D. F., Cordes J. M., 2002, ApJ, 568, 289
Asaoka I., Aschenbach B., 1994, A&A, 284, 573
Bailer-Jones C. A. L., Rybizki J., Fouesneau M., Demleitner M., Andrae R., 2021, AJ, 161, 147
Bietenholz M. F., Kondratiev V., Ransom S., Slane P., Bartel N., Buchner S., 2013, MNRAS, 431, 2590
Blaauw A., 1961, Bull. Astron. Inst. Netherlands, 15, 265
Blair W. P., Sawyer D. L., Kirshner R. P., Gull T. R., Parker R. A. R., 1980, ApJ, 242, 592
Bocchino F., Bykov A. M., 2001, A&A, 376, 248
Bocchino F., Miceli M., Troja E., 2009, A&A, 498, 139
Boubert D., Fraser M., Evans N. W., Green D. A., Izzard R. G., 2017, A&A, 606, A14
Boumis P., Mavromatakis F., Xilouris E. M., Alikakos J., Redman M. P., Goudis C. D., 2005, A&A, 443, 175
Burrows D. N., Guo Z., 1994, ApJ, 421, L19
Camilo F. et al., 2002, ApJ, 571, L41
Cannon A. J., Mayall M. W., 1949, Ann. Harvard College Obs., 112, 1
Cardelli J. A., Clayton G. C., Mathis J. S., 1989, ApJ, 345, 245
Chen Y., Bressan A., Girardi L., Marigo P., Kong X., Lanza A., 2015, MNRAS, 452, 1068
Chevalier R. A., 1999, ApJ, 511, 798
Chini R., Wink J. E., 1984, A&A, 139, L5
Clark D. H., Murdin P., Wood R., Gilmozzi R., Danziger J., Furr A. W., 1983, MNRAS, 204, 415
Claussen M. J., Frail D. A., Goss W. M., Gaume R. A., 1997, ApJ, 489, 143
Cordes J. M., Lazio T. J. W., 2002, preprint (arXiv:e-prints)
Crawford D., Limber D. N., Mendoza E., Schulte D., Steinman H., Swihart T., 1955, ApJ, 121, 24
Cutri R. M. et al., 2003, VizieR Online Data Catalog, p. II/246
Davidson K., Fesen R. A., 1985, ARA&A, 23, 119
Dib R., Kaspi V. M., 2014, ApJ, 784, 37
Dinçel B., Neuhäuser R., Yerli S. K., Ankay A., Tetzlaff N., Torres G., Mugrauer M., 2015, MNRAS, 448, 3196
Duncan R. C., Thompson C., 1992, ApJ, 392, L9
Fesen R. A. et al., 2006, ApJ, 645, 283
Fesen R. A., 1984, ApJ, 281, 658
Fesen R. A., Blair W. P., Kirshner R. P., 1985, ApJ, 292, 29
Fesen R. A., Downes R. A., Wallace D., Normandeau M., 1995, AJ, 110, 2876
Fesen R. A., Kirshner R. P., 1980, ApJ, 242, 1023
Fesen R. A., Shull J. M., Hurford A. P., 1997a, AJ, 113, 354
Fesen R. A., Winkler F., Rathore Y., Downes R. A., Wallace D., Tweedy R. W., 1997b, AJ, 113, 767
Fesen R., Rudie G., Hurford A., Soto A., 2008, ApJS, 174, 379
Fich M., 1986, ApJ, 303, 465
Foster T., Brunt C. M., 2015, AJ, 150, 147
Foster T., MacWilliams J., 2006, ApJ, 644, 214
Fraser M., Boubert D., 2019, ApJ, 871, 92
Gaensler B. M., Slane P. O., 2006, ARA&A, 44, 17
Gaia Collaboration, Vallenari A., Brown A.G.A, et al., 2023j, A&A, 674, A1
Gaia Collaboration, Prusti T., et al., 2016b, A&A, 595, A1
Galt J. A., Kennedy J. E. D., 1968, AJ, 73, 135
Georgelin Y. M., Georgelin Y. P., Roux S., 1973, A&A, 25, 337
Gies D. R., Bolton C. T., 1986, ApJS, 61, 419
Girardi L. et al., 2008, PASP, 120, 583
Gkouvelis L., Fabregat J., Zorec J., Steeghs D., Drew J. E., Raddi R., Wright N. J., Drake J. J., 2016, A&A, 591, A140
Green D. A., 2009, VizieR Online Data Catalog, 7253, 0
Guo Z., Burrows D. N., 1997, ApJ, 480, L51
Guseinov O. H., Ankay A., Sezer A., Tagieva S. O., 2003, Astron. Astrophys. Trans., 22, 273
Guseinov O. H., Ankay A., Tagieva S. O., 2005, Astrophysics, 48, 330(G05)
Hailey C. J., Craig W. W., 1994, ApJ, 434, 635
Hambaryan V. et al., 2022, MNRAS, 511, 4123
Hardorp J., Rohlfs K., Slettebak A., Stock J., 1959, Hamburger Sternw. Warner and Swasey Obs., C01, 0
Hirschauer A., Federman S. R., Wallerstein G., Means T., 2009, ApJ, 696, 1533
Hobbs G., Lorimer D. R., Lyne A. G., Kramer M., 2005, MNRAS, 360, 974
Hughes J. P., Rakowski C. E., Burrows D. N., Slane P. O., 2000, ApJ, 528, L109
Humphreys R. M., 1978, ApJS, 38, 309
Hurford A. P., Fesen R. A., 1996, ApJ, 469, 246
Johnson H. L., Morgan W. W., 1953, ApJ, 117, 313
Joncas G., Roger R. S., Dewdney P. E., 1989, A&A, 219, 303
Joshi Y. C., Balona L. A., Joshi S., Kumar B., 2014, MNRAS, 437, 804
Kaper L., van Loon J. T., Augusteijn T., Goudfrooij P., Patat F., Waters L. B. F. M., Zijlstra A. A., 1997, ApJ, 475, L37
Kaplan D. L., Chatterjee S., Gaensler B. M., Anderson J., 2008, ApJ, 677, 1201
Kaspi V. M., Gavriil F. P., Woods P. M., Jensen J. B., Roberts M. S. E., Chakrabarty D., 2003, ApJ, 588, L93
Kawasaki M., Ozaki M., Nagase F., Inoue H., Petre R., 2005, ApJ, 631, 935
Kiminki M. M., Kim J. S., Bagley M. B., Sherry W. H., Rieke G. H., 2015, ApJ, 813, 42
Kirshner R. P., Chevalier R. A., 1978, Nature, 276, 480
Kochanek C. S., 2018, MNRAS, 473, 1633
Kochanek C. S., 2021, MNRAS, 507, 5832
Koenig X. P., Leisawitz D. T., 2014, ApJ, 791, 131
Kokusho T., Nagayama T., Kaneda H., Ishihara D., Lee H.-G., Onaka T., 2013, ApJ, 768, L8
Koralesky B., Frail D. A., Goss W. M., Claussen M. J., Green A. J., 1998, AJ, 116, 1323
Kothes R., 2013, A&A, 560, A18
Kothes R., Fedotov K., Foster T. J., Uyanıker B., 2006, A&A, 457, 1081
Kothes R., Foster T., 2012, ApJ, 746, L4
Kothes R., Uyaniker B., Yar A., 2002, ApJ, 576, 169
Kramer M., Lyne A. G., Hobbs G., Löhmer O., Carr P., Jordan C., Wolszczan A., 2003, ApJ, 593, L31
Landecker T. L., Pineault S., Routledge D., Vaneldik J. F., 1989, MNRAS, 237, 277
Landecker T. L., Roger R. S., Dewdney P. E., 1982, AJ, 87, 1379
Lazendic J. S., Dewey D., Schulz N. S., Canizares C. R., 2006, ApJ, 651, 250
Lazendic J. S., Slane P. O., 2006, ApJ, 647, 350
Leahy D. A., 2004, AJ, 127, 2277
Leahy D. A., Aschenbach B., 1995, A&A, 293, 853
Leahy D. A., Tian W. W., 2007, A&A, 461, 1013
Leahy D., Tian W., 2006, A&A, 451, 251
Lesh J. R., Aizenman M. L., 1973, A&A, 22, 229
Livingstone M. A., Ransom S. M., Camilo F., Kaspi V. M., Lyne A. G., Kramer M., Stairs I. H., 2009, ApJ, 706, 1163
Lozinskaia T. A., 1979a, Aust. J. Phys., 32, 113
Lozinskaia T. A., 1979b, A&A, 71, 29
Lozinskaia T. A., 1980, A&A, 84, 26
Lozinskaya T. A., 1969, Soviet Ast., 13, 192
Lozinskaya T. A., 1981, Sov. Astron. Lett., 7, 29
Lux O., Neuhäuser R., Mugrauer M., Bischoff R., 2021, Astron. Nachr., 342, 553
Lyne A. G., Jordan C. A., Graham-Smith F., Espinoza C. M., Stappers B. W., Weltevrede P., 2015, MNRAS, 446, 857
Lyne A. G., Lorimer D. R., 1994, Nature, 369, 127
MacAlpine G. M., Satterfield T. J., 2008, AJ, 136, 2152
MacAlpine G. M., Uomoto A., 1991, AJ, 102, 218
Maíz Apellániz J. et al., 2016, ApJS, 224, 4
Maíz Apellániz J., 2010, A&A, 518, A1
Martin N., 1972, A&A, 17, 253

Mavromatakis F., Boumis P., Paleologou E. V., 2002, A&A, 383, 1011
McGowan K. E., Zane S., Cropper M., Vestrand W. T., Ho C., 2006, ApJ, 639, 377
McKee C. F., Ostriker J. P., 1977, ApJ, 218, 148
Mel'Nik A. M., Efremov Y. N., 1995, Astron. Lett., 21, 10
Miller J. S., 1973, ApJ, 180, L83
Mitra D., Wielebinski R., Kramer M., Jessner A., 2003, A&A, 398, 993
Morgan W. W., Code A. D., Whitford A. E., 1955, ApJS, 2, 41
Morgan W. W., Keenan P. C., Kellman E., 1943, An Atlas of Stellar Spectra, with an Outline of Spectral Classification. The University of Chicago press, USA
Mugrauer M., Avila G., Guirao C., 2014, Astron. Nachr., 335, 417
Murray S. S., Slane P. O., Seward F. D., Ransom S. M., Gaensler B. M., 2002, ApJ, 568, 226
Negueruela I., Marco A., 2003, A&A, 406, 119
Negueruela I., Steele I. A., Bernabeu G., 2004, Astron. Nachr., 325, 749
Neuhäuser R., Gießler F., Hambaryan V. V., 2020, MNRAS, 498, 899
Neuhäuser R., Torres G., Mugrauer M., Neuhäuser D. L., Chapman J., Luge D., Cosci M., 2022, MNRAS, 516, 693
O'Donnell J. E., 1994, ApJ, 422, 158
Oey M. S., Watson A. M., Kern K., Walth G. L., 2005, AJ, 129, 393
Olbert C. M., Clearfield C. R., Williams N. E., Keohane J. W., Frail D. A., 2001, ApJ, 554, L205
Oskinova L. M., Gvaramadze V. V., Gräfener G., Langer N., Todt H., 2020, A&A, 644, L8
Pannuti T. G., Rho J., Borkowski K. J., Cameron P. B., 2010, AJ, 140, 1787
Pavlov G. G., Luna G. J. M., 2009, ApJ, 703, 910
Petre R., Szymkowiak A. E., Seward F. D., Willingale R., 1988, ApJ, 335, 215
Pflamm-Altenburg J., Kroupa P., 2010, MNRAS, 404, 1564
Philp C. J., Evans C. R., Leonard P. J. T., Frail D. A., 1996, AJ, 111, 1220
Pineault S., Landecker T. L., Routledge D., 1987, ApJ, 315, 580
Poveda A., Ruiz J., Allen C., 1967, Boletin de los Observatorios Tonantzintla y Tacubaya, 4, 86
Poveda A., Woltjer L., 1968, AJ, 73, 65
Przybilla N., Nieva M. F., Heber U., Butler K., 2008, ApJ, 684, L103
Ramírez Alegría S., Herrero A., Marín-Franch A., Puga E., Najarro F., Acosta Pulido J. A., Hidalgo S. L., Simón-Díaz S., 2011, A&A, 535, A8
Read P. L., 1981, MNRAS, 194, 863
Reed J. E., Hester J. J., Fabian A. C., Winkler P. F., 1995, ApJ, 440, 706
Reich W., Braunsfurth E., 1981, A&A, 99, 17
Renzo M. et al., 2019, A&A, 624, A66
Rest A. et al., 2011, ApJ, 732, 3
Rho J., Petre R., 1998, ApJ, 503, L167
Ritter A., Parker Q. A., Lykou F., Zijlstra A. A., Guerrero M. A., Le Dû P., 2021, ApJ, 918, L33
Roberts D. A., Goss W. M., Kalberla P. M. W., Herbstmeier U., Schwarz U. J., 1993, A&A, 274, 427
Routledge D., Dewdney P. E., Landecker T. L., Vaneldik J. F., 1991, A&A, 247, 529
Russeil D., Adami C., Georgelin Y. M., 2007, A&A, 470, 161
Sasaki M., Kothes R., Plucinsky P. P., Gaetz T. J., Brunt C. M., 2006, ApJ, 642, L149
Sasaki M., Plucinsky P. P., Gaetz T. J., Bocchino F., 2013, A&A, 552, A45
Sayer R. W., Nice D. J., Kaspi V. M., 1996, ApJ, 461, 357
Slane P. O., Helfand D. J., Murray S. S., 2002, ApJ, 571, L45
Snell R. L., Hollenbach D., Howe J. E., Neufeld D. A., Kaufman M. J., Melnick G. J., Bergin E. A., Wang Z., 2005, ApJ, 620, 758
Sota A., Maíz Apellániz J., Walborn N. R., Alfaro E. J., Barbá R. H., Morrell N. I., Gamen R. C., Arias J. I., 2011, ApJS, 193, 24
Stephenson F. R., Green D. A., 2002, Historical Supernovae and Their Remnants. International Series in Astronomy and Astrophysics, Vol. 5. Clarendon Press, Oxford
Suad L. A., Cichowolski S., Noriega-Crespo A., Arnal E. M., Testori J. C., Flagey N., 2016, A&A, 585, A154
Swartz D. A. et al., 2015, ApJ, 808, 84
Tammann G. A., Loeffler W., Schroeder A., 1994, ApJS, 92, 487
Tatematsu K., Fukui Y., Iwata T., Seward F. D., Nakano M., 1990, ApJ, 351, 157
Tauris T. M., Takens R. J., 1998, A&A, 330, 1047
Taylor J. H., Cordes J. M., 1993, ApJ, 411, 674
Tetzlaff N., Dinçel B., Neuhäuser R., Kovtyukh V. V., 2014, MNRAS, 438, 3587
Tetzlaff N., Eisenbeiss T., Neuhäuser R., Hohle M. M., 2011b, MNRAS, 417, 617
Tetzlaff N., Neuhäuser R., Hohle M. M., 2011a, MNRAS, 410, 190
Tian W. W., Leahy D. A., 2006, A&A, 447, 205
Tian W. W., Leahy D. A., Li D., 2010, MNRAS, 404, L1
Tody D., 1986, in Crawford D. L., ed., Proc. SPIE Conf. Ser. Vol. 627, Instrumentation in Astronomy VI. SPIE, Bellingham, p. 733
Trimble V., 1973, PASP, 85, 579
Troja E., Bocchino F., Miceli M., Reale F., 2008, A&A, 485, 777
van den Bergh S., 1980, JA&A, 1, 67
van den Heuvel E. P. J., 1993, Space Sci. Rev., 66, 309
van den Heuvel E. P. J., van Paradijs J., 1997, ApJ, 483, 399
Ward J. L., Kruijssen J. M. D., Rix H.-W., 2020, MNRAS, 495, 663
Welsh B. Y., Sallmen S., 2003, A&A, 408, 545
Wongwathanarat A., Janka H.-T., Müller E., 2013, A&A, 552, A126
Wright E. L. et al., 2010, AJ, 140, 1868
Xilouris K. M., Papamastorakis J., Paleologou E. V., Andredakis Y., Haerendel G., 1993, A&A, 270, 393
Xu Y., Reid M. J., Zheng X. W., Menten K. M., 2006, Science, 311, 54
Yao J. M., Manchester R. N., Wang N., 2017, 835, 29
Yao J. M., Manchester R. N., Wang N., 2017, ApJ, 835, 29
Yar-Uyaniker A., Uyaniker B., Kothes R., 2004, ApJ, 616, 247
Yuan J. P., Manchester R. N., Wang N., Zhou X., Liu Z. Y., Gao Z. F., 2010, ApJ, 719, L111
Zhu W., Kaspi V. M., Dib R., Woods P. M., Gavriil F. P., Archibald A. M., 2008, ApJ, 686, 520

APPENDIX A: FOURIER CROSS-CORRELATION

Fourier cross-correlation of the star TYC 3572-00017-1 with an F0V and a B2V type star is given in Fig. A1.

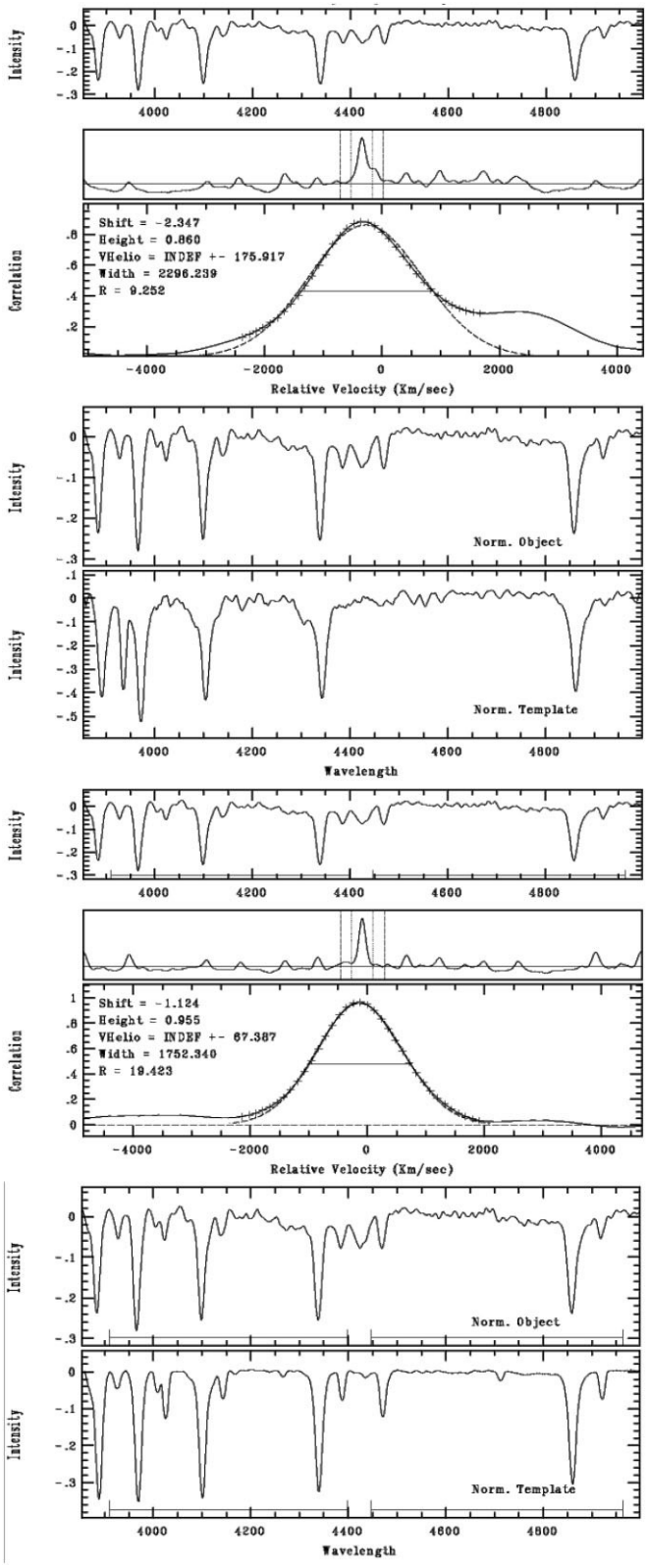

Figure A1. *From top to bottom*: Fourier cross-correlation of TYC 3572-00017-1 with an F0V type star. Scaled spectra of the star and the template. Fourier cross-correlation of the same with a smoothed B2V-type MK standard star. Scaled spectra of the star and the template.

APPENDIX B: ISM ABSORPTION LINES

ISM absorption lines of HD 8768 and HD 278115 are shown in Figs. B1–B3.

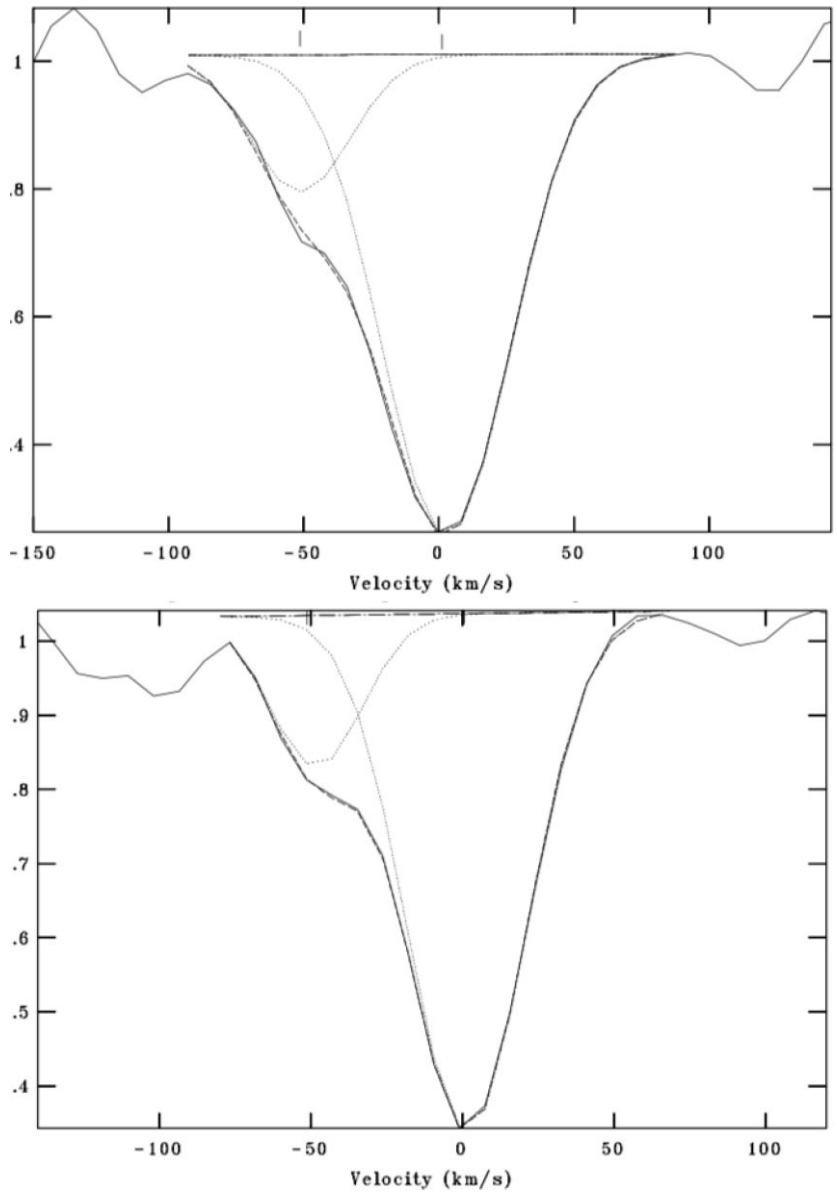

Figure B1. FLECHAS spectrum of HD 8768. Blue-shifted ISM sodium Na D1 and D2 lines towards the star HD 8768. The relative radial velocity of the gas is $\sim$−50 km s^{-1}. It might have been accelerated by the SNR.

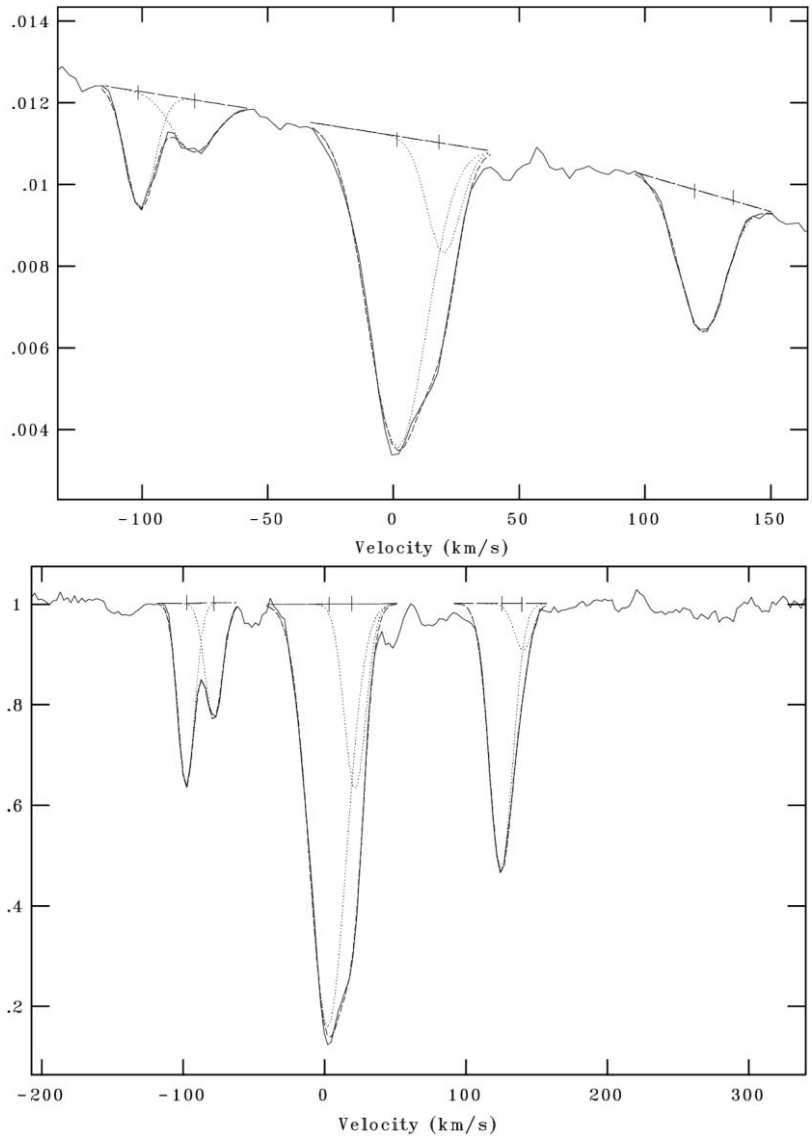

Figure B2. The high-velocity components to the ISM Ca II and K and H lines detected on the TRES spectrum of HD 278115. The reference (zero velocity) is chosen as the strongest absorption line corresponding to the total column density between the source and the observer.

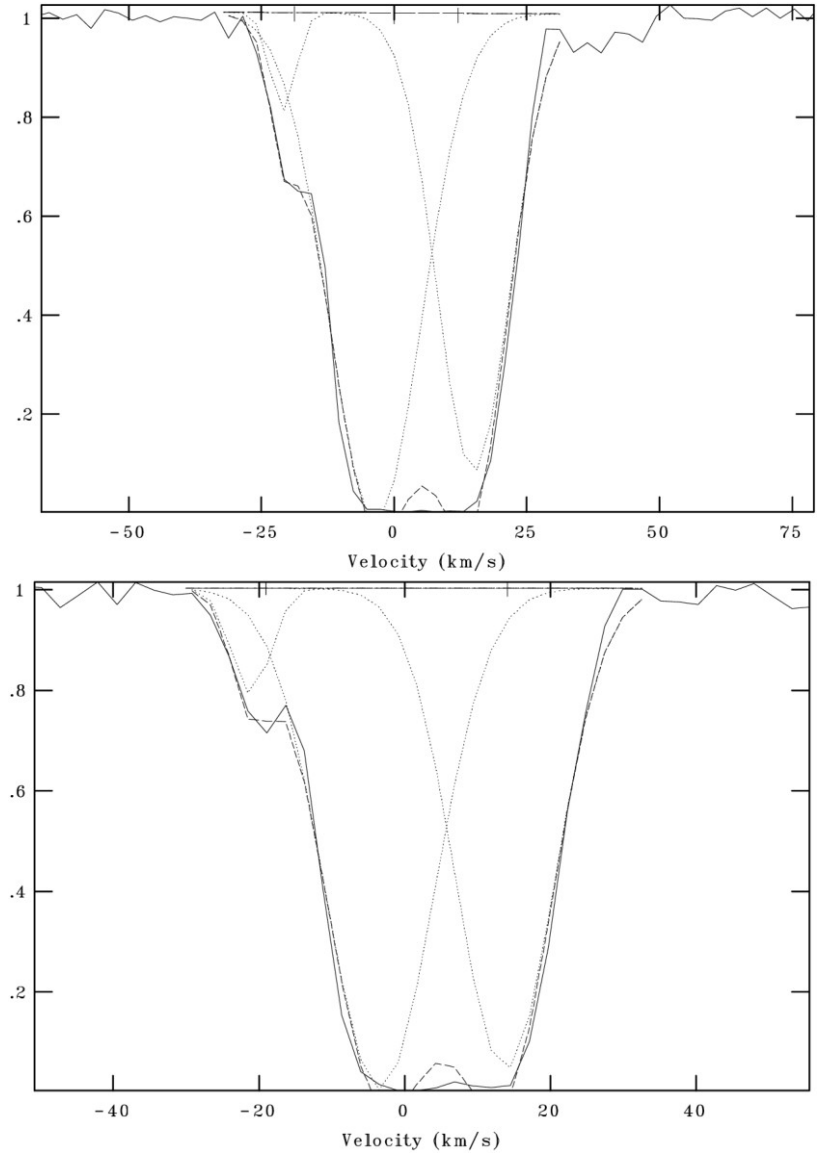

Figure B3. The high-velocity components to the ISM Na I–D1 and D2 lines detected on the TRES spectrum of HD 278115. The reference (zero velocity) is chosen as the strongest absorption line corresponding to the total column density between the source and the observer.

APPENDIX C: LIST OF STARS

In this section, the list of the stars of which spectra were taken for this work (Table C1), and a list of reference stars (Table C2).

Table C1. List of stars observed.

RA	Dec.	G (mag)	G_{BP}–G_{RP} (mag)	Instr.	A_V	Dist. (pc)	SpT	SNR
00 00 29.61	+62 16 20.97	12.11	0.38	C	$1.14^{+0.08}_{-0.10}$	1273^{+16}_{-19}	B9V	G116.9 + 0.2
00 01 01.34	+62 21 52.76	12.67	0.44	C	$1.30^{+0.08}_{-0.10}$	1551^{+26}_{-26}	B9V	G116.9 + 0.2
23 58 00.99	+62 28 29.34	12.74	0.43	C	$1.28^{+0.08}_{-0.10}$	1772^{+39}_{-35}	B9V	G116.9 + 0.2
23 58 37.52	+62 27 59.04	12.82	0.32	C	$1.33^{+0.01}_{-0.05}$	2204^{+72}_{-75}	B5V	G116.9 + 0.2
23 58 40.65	+62 21 18.87	13.66	0.63	C	$1.41^{+0.04}_{-0.02}$	2131^{+51}_{-59}	A2V	G116.9 + 0.2
23 59 06.16	+62 20 01.31	12.77	0.43	C	$1.60^{+0.01}_{-0.05}$	2523^{+97}_{-90}	B5V	G116.9 + 0.2
23 59 11.31	+62 30 49.82	13.77	0.59	C	$1.31^{+0.04}_{-0.02}$	1734^{+48}_{-48}	A2V	G116.9 + 0.2
23 59 13.15	+62 23 04.52	13.80	0.83	C	$1.12^{+0.05}_{-0.05}$	1498^{+33}_{-31}	F0V	G116.9 + 0.2
23 59 18.37	+62 28 41.84	13.03	0.61	C	$0.59^{+0.05}_{-0.05}$	3562^{+180}_{-134}	F0V	G116.9 + 0.2
23 59 24.10	+62 30 22.80	13.26	0.46	C	$0.99^{+0.04}_{-0.02}$	1492^{+22}_{-28}	A2V	G116.9 + 0.2
23 59 24.94	+62 29 03.78	13.19	0.47	C	$1.36^{+0.08}_{-0.10}$	2679^{+127}_{-110}	B9V	G116.9 + 0.2
23 59 24.67	+62 20 47.25	9.371	0.38	C	$1.14^{+0.08}_{-0.10}$	555^{+4}_{-4}	B9V	G116.9 + 0.2
23 59 29.44	+62 30 44.18	12.24	0.44	C	$1.01^{+0.08}_{-0.02}$	963^{+12}_{-12}	A1V	G116.9 + 0.2
23 59 38.96	+62 35 19.25	12.67	0.41	C	$1.43^{+0.03}_{-0.05}$	3068^{+162}_{-118}	B7V	G116.9 + 0.2
23 59 42.23	+62 18 22.07	12.20	0.42	C	$1.61^{+0.03}_{-0.03}$	3112^{+123}_{-107}	B4V	G116.9 + 0.2
02 16 52.10	+62 39 58.79	13.66	1.02	C	$1.77^{+0.05}_{-0.05}$	1506^{+30}_{-31}	A8V	G132.7 + 1.3
02 17 08.26	+62 57 18.67	11.43	0.56	C	$1.78^{+0.03}_{-0.05}$	940^{+27}_{-26}	B7V	G132.7 + 1.3
02 17 12.37	+62 51 51.08	13.47	0.78	C	$2.32^{+0.03}_{-0.05}$	2797^{+118}_{-125}	B7V	G132.7 + 1.3
02 17 17.69	+62 41 41.62	13.70	0.87	C	$1.76^{+0.06}_{-0.04}$	1275^{+19}_{-23}	A4V	G132.7 + 1.3
02 17 22.38	+62 53 52.43	12.20	0.90	C	$2.85^{+0.07}_{-0.05}$	2274^{+65}_{-54}	B3V	G132.7 + 1.3
02 18 00.23	+62 45 48.35	12.10	1.04	C	$1.24^{+0.02}_{-0.03}$	517^{+4}_{-5}	F5V	G132.7 + 1.3
02 18 00.44	+62 41 19.66	13.83	1.01	C	$2.10^{+0.06}_{-0.04}$	980^{+307}_{-167}	A4V	G132.7 + 1.3
02 18 25.74	+62 44 44.10	13.50	0.98	C	$2.72^{+0.04}_{-0.04}$	3337^{+148}_{-132}	B8V	G132.7 + 1.3
02 18 35.73	+62 43 49.75	12.26	0.68	C	$1.88^{+0.08}_{-0.10}$	1075^{+19}_{-15}	B9V	G132.7 + 1.3
02 18 39.98	+62 45 24.70	13.14	1.35	C	$1.88^{+0.07}_{-0.04}$	5749^{+477}_{-496}	F6e	G132.7 + 1.3
02 19 29.61	+62 43 31.08	13.06	1.27	C	$1.78^{+0.02}_{-0.03}$	644^{+10}_{-9}	F5V	G132.7 + 1.3
23 01 29.53	+58 53 57.53	13.41	0.64	C	$1.35^{+0.07}_{-0.06}$	2531^{+86}_{-64}	A3V	G109.1 − 1.0
23 01 32.52	+58 55 07.87	11.92	0.43	C	$0.99^{+0.08}_{-0.02}$	833^{+8}_{-7}	A1V	G109.1 − 1.0
23 01 45.68	+58 48 13.49	11.75	0.49	C	$0.98^{+0.07}_{-0.06}$	851^{+10}_{-8}	A3V	G109.1 − 1.0
23 01 50.70	+58 52 56.96	12.65	0.62	C	$1.29^{+0.07}_{-0.06}$	1234^{+15}_{-18}	A3V	G109.1 − 1.0
23 02 04.38	+58 52 44.06	11.69	0.43	T	$1.49^{+0.03}_{-0.05}$	2090^{+70}_{-63}	B7V	G109.1 − 1.0
23 02 10.65	+58 53 30.20	12.15	0.88	C	$1.14^{+0.05}_{-0.05}$	1164^{+14}_{-13}	F1V	G109.1 − 1.0
23 36 25.99	+62 03 58.30	11.69	0.99	T	$2.73^{+0.04}_{-0.04}$	1071^{+15}_{-13}	B8V	G114.3 + 0.3
23 37 09.18	+61 57 34.76	13.32	1.17	C	$2.62^{+0.07}_{-0.06}$	2054^{+39}_{-44}	A3V	G114.3 + 0.3
23 37 22.74	+61 40 23.92	10.73	0.68	T	$2.48^{+0.04}_{-0.08}$	1513^{+19}_{-23}	B2V	G114.3 + 0.3
23 38 08.38	+62 00 31.14	11.72	0.37	C	$0.95^{+0.08}_{-0.04}$	803^{+11}_{-12}	A0V	G114.3 + 0.3
23 38 43.57	+62 03 21.18	11.97	1.05	T	$3.03^{+0.02}_{-0.03}$	2883^{+70}_{-64}	B6V	G114.3 + 0.3
01 20 43.81	+64 15 56.61	11.58	0.86	C	$1.95^{+0.04}_{-0.02}$	712^{+7}_{-7}	A2V	G126.2 + 1.6
01 20 45.79	+64 23 53.04	11.51	0.76	C	$2.06^{+0.08}_{-0.10}$	772^{+8}_{-8}	B9V	G126.2 + 1.6
01 21 37.64	+64 12 37.21	12.76	1.33	C	$2.98^{+0.07}_{-0.06}$	1067^{+14}_{-12}	A3V	G126.2 + 1.6
01 22 08.61	+64 17 48.41	11.83	0.88	C	$1.15^{+0.05}_{-0.05}$	425^{+2}_{-3}	F1V	G126.2 + 1.6

Table C1 – *continued*

RA	Dec.	G (mag)	G_{BP}–G_{RP} (mag)	Instr.	A_V	Dist. (pc)	SpT	SNR
01 22 14.37	+64 17 58.15	12.55	1.03	T	$3.32^{+0.04}_{-0.08}$	4160^{+199}_{-207}	B2V	G126.2 + 1.6
01 22 29.95	+64 12 47.31	13.08	1.14	C	$1.30^{+0.04}_{-0.05}$	606^{+5}_{-4}	F7V	G126.2 + 1.6
01 22 39.39	+64 16 53.36	13.40	1.04	C	$3.42^{+0.06}_{-0.04}$	4624^{+296}_{-279}	B1V	G126.2 + 1.6
01 22 45.63	+64 07 11.09	13.23	1.25	C	$2.89^{+0.04}_{-0.02}$	774^{+8}_{-9}	A2V	G126.2 + 1.6
01 22 48.14	+64 18 52.83	13.16	1.21	C	$1.84^{+0.04}_{-0.04}$	728^{+7}_{-6}	F2V	G126.2 + 1.6
01 22 57.09	+64 12 29.66	11.33	0.74	C	$1.10^{+0.05}_{-0.05}$	404^{+3}_{-3}	A8V	G126.2 + 1.6
01 23 17.68	+64 09 17.60	12.92	1.26	C	$2.35^{+0.05}_{-0.05}$	889^{+10}_{-11}	A8V	G126.2 + 1.6
01 27 16.87	+63 08 55.85	11.25	1.05	C	$2.97^{+0.03}_{-0.05}$	1278^{+46}_{-53}	B7V	G127.1 + 0.5
01 27 49.51	+63 04 35.03	11.88	0.96	C	$2.25^{+0.08}_{-0.02}$	1031^{+15}_{-15}	A1V	G127.1 + 0.5
01 28 03.15	+63 16 57.18	8.681	0.59	C	$2.50^{+0.08}_{-0.12}$	8813^{+2241}_{-1728}	B0V	G127.1 + 0.5
01 28 12.40	+63 09 12.61	13.55	1.04	C	$2.40^{+0.04}_{-0.02}$	1066^{+15}_{-13}	A2V	G127.1 + 0.5
01 28 21.17	+63 13 12.50	10.97	0.66	T	$1.94^{+0.04}_{-0.04}$	275^{+45}_{-32}	B8V	G127.1 + 0.5
01 28 36.68	+63 12 28.04	13.81	0.93	C	$2.18^{+0.08}_{-0.02}$	2006^{+57}_{-52}	A1V	G127.1 + 0.5
04 59 09.98	+46 53 35.96	10.60	0.30	C	$0.77^{+0.08}_{-0.04}$	514^{+5}_{-5}	A0V	G160.9 + 2.6
04 59 17.52	+46 47 15.68	10.76	0.30	C	$0.78^{+0.08}_{-0.04}$	621^{+6}_{-6}	A0V	G160.9 + 2.6
05 00 31.29	+46 33 27.25	11.07	0.76	C	$1.77^{+0.08}_{-0.02}$	1010^{+19}_{-17}	A1V	G160.9 + 2.6
05 00 53.98	+46 30 00.61	11.39	0.79	C	$1.68^{+0.07}_{-0.06}$	920^{+17}_{-16}	A3V	G160.9 + 2.6
05 01 16.00	+46 33 21.68	10.87	0.55	C	$1.19^{+0.04}_{-0.02}$	600^{+5}_{-6}	A2V	G160.9 + 2.6
05 03 00.98	+46 39 44.12	10.83	0.25	C	$0.66^{+0.08}_{-0.04}$	639^{+13}_{-12}	A0V	G160.9 + 2.6
05 25 37.19	+42 56 52.49	13.53	0.62	C	$1.53^{+0.08}_{-0.04}$	2350^{+86}_{-76}	A0V	G166.0 + 4.3
05 25 55.72	+42 48 27.80	13.25	0.73	C	$1.54^{+0.07}_{-0.06}$	2854^{+113}_{-97}	A3V	G166.0 + 4.3
05 26 01.35	+42 58 03.78	13.46	0.77	C	$2.07^{+0.08}_{-0.10}$	3047^{+165}_{-132}	B9V	G166.0 + 4.3
05 26 24.90	+42 53 49.81	12.09	0.66	C	$1.63^{+0.08}_{-0.04}$	1777^{+98}_{-95}	A0V	G166.0 + 4.3
05 26 33.92	+42 53 08.70	14.93	0.73	F	$2.10^{+0.06}_{-0.06}$	4282^{+465}_{-409}	A3IV	G166.0 + 4.3
05 26 37.39	+43 00 29.77	13.77	0.75	C	$0.99^{+0.07}_{-0.04}$	1110^{+22}_{-17}	A9V	G166.0 + 4.3
05 26 37.52	+43 01 10.96	10.02	0.41	T	$2.07^{+0.08}_{-0.12}$	3955^{+248}_{-220}	B0.5V	G166.0 + 4.3
05 26 41.60	+43 02 29.06	13.02	0.72	C	$0.58^{+0.04}_{-0.05}$	752^{+8}_{-9}	F3V	G166.0 + 4.3
05 26 48.82	+43 00 40.53	12.28	0.39	C	$1.17^{+0.08}_{-0.10}$	2643^{+175}_{-138}	B9V	G166.0 + 4.3
05 27 00.12	+42 49 42.71	12.73	0.73	C	$0.49^{+0.02}_{-0.03}$	632^{+28}_{-26}	F5V	G166.0 + 4.3
05 27 02.94	+42 51 47.59	13.76	0.97	C	$1.12^{+0.02}_{-0.05}$	2216^{+144}_{-87}	F4V	G166.0 + 4.3
06 16 24.86	+22 26 25.35	12.24	0.42	C	$0.96^{+0.08}_{-0.02}$	969^{+14}_{-14}	A1V	G189.1 + 3.0
06 16 39.29	+22 27 50.00	12.87	0.58	C	$0.51^{+0.05}_{-0.05}$	1258^{+31}_{-43}	F0V	G189.1 + 3.0
06 16 48.47	+22 31 57.41	12.61	0.56	T	$1.22^{+0.04}_{-0.02}$	943^{+20}_{-15}	A2V	G189.1 + 3.0
06 16 53.35	+22 44 27.29	11.73	1.29	C	$3.93^{+0.04}_{-0.08}$	1704^{+75}_{-62}	B2V	G189.1 + 3.0
06 16 54.81	+22 40 39.18	12.63	1.03	C	$1.24^{+0.02}_{-0.05}$	1219^{+26}_{-24}	F4V	G189.1 + 3.0
06 16 56.27	+22 29 46.64	12.52	0.57	T	$1.30^{+0.08}_{-0.02}$	838^{+32}_{-26}	A1V	G189.1 + 3.0
06 16 58.80	+22 35 58.47	13.05	1.39	C	$4.00^{+0.07}_{-0.05}$	1699^{+43}_{-44}	B3V	G189.1 + 3.0
06 17 07.86	+22 42 20.32	12.80	1.06	C	$3.10^{+0.01}_{-0.05}$	1637^{+58}_{-48}	B5V	G189.1 + 3.0
06 17 31.70	+22 24 56.77	13.24	0.82	C	$2.46^{+0.02}_{-0.03}$	1716^{+48}_{-43}	B6V	G189.1 + 3.0

Table C2. List of reference stars.

RA	Dec.	Dist	SNR	SpT	G (mag)	$J-K$	$W2-W3$	$W3-W4$
02 26 34.39	+62 00 42.35	2039^{+70}_{-94}	G132.7 + 1.3	O6.5V((f))z (1)	9.92	0.36	2.13	3.62
02 26 34.87	+62 00 46.79	1972^{+70}_{-54}	G132.7 + 1.3	B (1)	12.87	0.65	–	–
02 26 49.63	+62 15 35.08	2070^{+95}_{-94}	G132.7 + 1.3	O6V + O? (2)	12.95	1.2	–	–
22 55 42.27	+58 28 23.84	2881^{+119}_{-96}	G109.1 − 1.0	–	13.62	0.67	2.9	4.54
22 56 17.45	+58 31 17.44	3269^{+323}_{-229}	G109.1 − 1.0	–	14.19	–	–	–
22 58 40.80	+58 46 59.18	3361^{+247}_{-202}	G109.1 − 1.0	O8.5V (4)	12.2	0.57	–	–
22 59 13.70	+58 44 42.92	2917^{+108}_{-99}	G109.1 − 1.0	O9/9.5V (4)	11.22	0.17	2.98	4.3
22 59 28.36	+58 47 51.12	3104^{+154}_{-140}	G109.1 − 1.0	B0.3V (3)	12.02	0.22	2.6	4.14
23 15 34.15	+61 47 47.64	2772^{+222}_{-202}	G114.3 + 0.3	–	15.61	1.1	–	–
23 15 49.16	+61 07 59.50	2729^{+82}_{-77}	G114.3 + 0.3	O9V (4)	11.7	0.43	3.93	4.37
23 16 27.73	+61 06 35.21	2752^{+669}_{-349}	G114.3 + 0.3	–	15.58	1.09	2.5	4.19
23 16 50.23	+61 40 53.78	2634^{+116}_{-114}	G114.3 + 0.3	–	14.66	0.94	3.45	5.06
23 16 50.52	+61 26 15.38	2783^{+79}_{-78}	G114.3 + 0.3	–	11.88	0.38	2.16	4.77
23 20 44.50	+61 11 40.53	2829^{+133}_{-100}	G114.3 + 0.3	O6.5f(n)p (5)	8.52	0.23	–	–
23 33 32.50	+60 47 32.04	2956^{+96}_{-95}	G114.3 + 0.3	O8V (4)	13.23	0.72	3.75	4.18
23 33 36.84	+60 45 07.38	2989^{+102}_{-95}	G114.3 + 0.3	O9V (4)	12.28	0.61	3.12	4.57
23 42 11.25	+60 56 35.75	3257^{+162}_{-131}	G114.3 + 0.3	–	11.96	0.4	0.44	3.93
01 23 07.04	+61 51 52.76	914^{+7}_{-8}	G127.1 + 0.5	B2.5V (4)	13.09	0.7	3.55	5.61
01 28 03.50	+63 17 02.55	2695^{+348}_{-243}	G127.1 + 0.5	–	15.37	–	–	–
01 28 40.55	+63 27 37.65	2478^{+205}_{-188}	G127.1 + 0.5	–	14.05	2.14	2.86	2.13
01 28 44.15	+63 27 11.38	2573^{+175}_{-143}	G127.1 + 0.5	–	15.62	2.01	2.44	2.4
01 30 11.13	+63 20 24.31	2807^{+455}_{-297}	G127.1 + 0.5	–	15.18	1.3	4.11	2.06
01 31 30.50	+63 09 14.31	2403^{+170}_{-161}	G127.1 + 0.5	B6/7V (6)	15.12	1.4	3.46	2.3
01 21 52.05	+64 15 06.09	4379^{+298}_{-274}	G126.2 + 1.6	A0Ib (7)	10.25	0.54	0.03	0.35
00 02 22.70	+62 54 03.16	4559^{+647}_{-593}	G116.9 + 0.2	B0.5III (3)	9.81	0.01	−0.02	0.38
00 04 25.06	+63 03 12.64	3190^{+139}_{-140}	G116.9 + 0.2	O9.5V (8)	11.12	0.13	0.03	0.71
05 27 16.15	+42 17 47.04	3889^{+438}_{-308}	G166.0 + 4.3	B3 (9)	9.36	0.19	0.38	2.52
06 16 58.70	+23 44 27.26	1746^{+93}_{-105}	G189.1 + 3.0	B2Ib (10)	6.11	0.21	−0.17	0.21
06 17 26.19	+22 25 36.95	1579^{+64}_{-54}	G189.1 + 3.0	Early B (16)	10.17	−0.16	−0.13	0.98
06 17 54.39	+22 24 32.92	1701^{+55}_{-54}	G189.1 + 3.0	B0.5 II-III (14)	8.76	0.41	0.01	0.2
06 18 00.35	+22 39 29.99	1852^{+72}_{-78}	G189.1 + 3.0	B0IIInk (11)	8.63	0.2	−0.12	−0.46
06 18 31.77	+22 40 45.05	2254^{+1594}_{-1162}	G189.1 + 3.0	O9V (10)	8.63	0.32	−0.06	0.3
06 18 39.43	+23 00 28.51	1766^{+59}_{-65}	G189.1 + 3.0	B1IV:p (12)	8.49	0.2	0.05	0.39
06 18 59.70	+23 00 04.05	1875^{+82}_{-98}	G189.1 + 3.0	B0.5II-III (13)	7.8	0.12	−0.02	0.32
06 19 19.29	+23 28 09.84	1989^{+118}_{-101}	G189.1 + 3.0	B0II (11)	6.81	0.14	−0.01	0.26
04 56 04.09	+47 22 35.04	4256^{+779}_{-502}	G160.9 + 2.6	–	15.62	0.67	–	–
04 56 10.59	+47 23 35.42	4157^{+316}_{-278}	G160.9 + 2.6	B1V (4)	11.89	0.24	2.56	4.82
04 58 30.87	+47 58 24.75	3940^{+450}_{-318}	G160.9 + 2.6	B2.5V (15)	14.73	0.14	–	–
04 58 45.33	+47 59 56.11	3885^{+286}_{-287}	G160.9 + 2.6	O9.5V (4)	11.21	0.13	3.67	4.39
05 01 24.24	+46 48 47.66	3801^{+477}_{-451}	G160.9 + 2.6	–	15.35	2.3	2.34	1.95

Note. (1) Maíz Apellániz et al. (2016); (2) Oey et al. (2005); (3) Negueruela & Marco (2003); (4) Russeil, Adami & Georgelin (2007); (5) Sota et al. (2011); (6) Gkouvelis et al. (2016); (7) Hardorp et al. (1959); (8) Martin (1972); (9) Cannon & Mayall (1949); (10) Negueruela, Steele & Bernabeu (2004); (11) Morgan, Code & Whitford (1955); (12) Lesh & Aizenman (1973); (13) Johnson & Morgan (1953); (14) Crawford et al. (1955); (15) Chini & Wink (1984); (16) this work.

This paper has been typeset from a TEX/LATEX file prepared by the author.